



Norwegian University of
Science and Technology

Characterisation of acoustic oscillations in annular systems

David Kieffer

Master's Thesis

Submission date: June 2016

Supervisor: Nicholas Worth, EPT

Norwegian University of Science and Technology
Department of Energy and Process Engineering

MASTER THESIS

Characterisation of acoustic oscillations in annular systems

submitted in partial fulfillment of the requirements

for the degree of

Master of Science

under the supervision of

Ass.Prof. Nicholas Worth

Ao.Univ.Prof. Dipl.-Ing. Dr.techn. Horst Ecker

submitted at NTNU

in cooperation with

Vienna University of Technology

by

David Kieffer

Stud.nr. 764810

Matr.nr. 0927368

Trondheim, 1st June 2016

.....

(David Kieffer)

EPT-M-2016-161

MASTER THESIS

for

Student David Kieffer

Spring 2016

Characterisation of Acoustic Oscillations in Annular systems**Background and objective**

Gas turbine engines are widely used to provide propulsion in aircraft and for power generation on land and sea. Currently engine manufacturers are working to reduce the emission of environmentally harmful combustion products by operating these engines under lean conditions (with more air than is needed for complete combustion). However, such operating conditions can make the combustion process unstable, resulting in large potentially damaging pressure and heat release oscillations, which need to be understood. This project aims to improve our understanding of this unstable process by making experimental measurements in a model annular combustor (modern gas turbines almost exclusively use annular architecture).

The project will involve dynamically controlling a number of loudspeakers, and the analysis of pressure measurements (using Labview and Matlab) to determine the modes and amplitudes of oscillation. The project will therefore be a mix of both experimental, analytical, and computational work, providing a broad range of skills and experience, and the chance to work on the cutting edge of fluids research.

The following tasks are to be considered:*Literature review*

1. Background reading and literature review of thermoacoustic instabilities in gas turbine combustors, including: why studying these is of interest in a practical sense; the dominant mechanisms responsible for these instabilities; the nature of pressure oscillations in annular chambers; how the current work fits into the wider framework of our current understanding.
2. Background reading and literature review of pressure measurements and relevant techniques such as the two-microphone method.

Microphone Calibration and setup

1. Design, build and use a loudspeaker testing chamber to calibrate multiple microphones in order to ensure that their pressure response is identical and derive transfer functions between them.
2. Demonstrate an understanding of the two-microphone technique in order to resolve components of pressure wave travelling in different directions around the annulus.

Control of oscillation pressure field using loudspeakers

1. Demonstrate the excitation of standing, spinning and mixed waves in the annular chamber.
2. Explore the parameters (relative loudspeaker forcing frequency, amplitude, phase) that control the pressure response in the annulus, and examine how to generate mixed modes.
3. Examine the effect of the number of loudspeakers used on the pressure response to answer the question – does increasing the number of loudspeakers make the response smoother?

Within 14 days of receiving the written text on the master thesis, the candidate shall submit a research plan for his project to the department.

When the thesis is evaluated, emphasis is put on processing of the results, and that they are presented in tabular and/or graphic form in a clear manner, and that they are analyzed carefully.

The thesis should be formulated as a research report with summary both in English and Norwegian, conclusion, literature references, table of contents etc. During the preparation of the text, the candidate should make an effort to produce a well-structured and easily readable report. In order to ease the evaluation of the thesis, it is important that the cross-references are correct. In the making of the report, strong emphasis should be placed on both a thorough discussion of the results and an orderly presentation.

The candidate is requested to initiate and keep close contact with his/her academic supervisor(s) throughout the working period. The candidate must follow the rules and regulations of NTNU as well as passive directions given by the Department of Energy and Process Engineering.

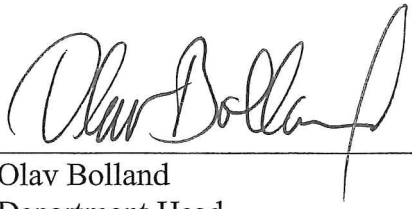
Risk assessment of the candidate's work shall be carried out according to the department's procedures. The risk assessment must be documented and included as part of the final report. Events related to the candidate's work adversely affecting the health, safety or security, must be documented and included as part of the final report. If the documentation on risk assessment represents a large number of pages, the full version is to be submitted electronically to the supervisor and an excerpt is included in the report.

Pursuant to “Regulations concerning the supplementary provisions to the technology study program/Master of Science” at NTNU §20, the Department reserves the permission to utilize all the results and data for teaching and research purposes as well as in future publications.

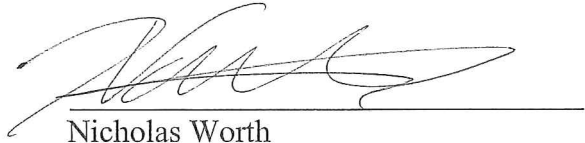
The final report is to be submitted digitally in DAIM. An executive summary of the thesis including title, student's name, supervisor's name, year, department name, and NTNU's logo and name, shall be submitted to the department as a separate pdf file. Based on an agreement with the supervisor, the final report and other material and documents may be given to the supervisor in digital format.

- Work to be done in lab (Water power lab, Fluids engineering lab, Thermal engineering lab)
 Field work

Department of Energy and Process Engineering, 14. January 2015



Olav Bolland
Department Head



Nicholas Worth
Academic Supervisor

Research Advisor:

Acknowledgements

The present work is the result of my second exchange during my studies. I am glad that I had the possibility to study in several countries. Most of all I want to thank my parents for enabling me to live this adventure. Their patience and moral support are the very basic fundament of this work. I also want to thank my friends for both discussing my work with me and distracting me from it, which helped me a lot to order my thoughts and recharge my batteries.

I also want to thank my supervisor Nicholas Worth for the possibility to work on such an interesting and multidisciplinary project and his patience as well as time to discuss the results and challenges of experimental work.

Last but not least, I want to thank Horst Ecker for raising my interest in noise and vibration control and encouraging me to write my thesis abroad.

Abstract

Gas turbine engines are widely used to provide propulsion in aircraft and for power generation on land and sea. Currently, engine manufacturers are working to reduce the emission of environmentally harmful combustion products by operating these engines under lean conditions (with more air than is needed for complete combustion). However, such operating conditions can make the combustion process unstable, resulting in large, potentially damaging pressure and heat release oscillations, which need to be understood. This project is aimed at improving our understanding of this unstable process by making experimental measurements in a model annular combustor (modern gas turbines almost exclusively use annular architecture).

The thesis work involves controlling a number of loudspeakers and the analysis of pressure measurements (using LabVIEW and MATLAB) to determine the modes and amplitudes of oscillation in an annular combustion chamber. The thesis therefore is a mix of experimental, analytical and computational work.

Recent research has shown that combustion instabilities in annular combustion chambers can lead to a mixture of standing and spinning azimuthal modes. The nature of these modes is not yet fully understood. The goal of this work is to demonstrate the excitation of standing, spinning and mixed modes in a cold, flow-less combustion chamber and to gain a better understanding of their nature.

Moderate control over the sound field in the annular system is demonstrated in the present work. While the excitation of standing waves is relatively simple, spinning modes could only partially be generated. It should be pointed out, however, that the methods applied seem to be promising if explored further and refined.

Kurzfassung

Gasturbinen sind heutzutage weit verbreitet, sei es in der Luftfahrt als Antrieb oder zur Energieumwandlung zu Land und in der Luft. Zuletzt bemühten sich die Hersteller die Abgaswerte zu verbessern. Der Betrieb bei Luftüberschuss, d.h. mit mehr Luft als für die Verbrennung eigentlich notwendig ist, hat sich dabei als hilfreich erwiesen. Allerdings treten bei solchen Betriebsbedingungen Verbrennungsinstabilitäten zutage. Die ungleichmäßige Verbrennung führt zu Schwankungen der Wärmefreisetzungsrate. Das verbrennende Gemisch in der Brennkammer dehnt sich bei Wärmefreigabe schlagartig aus. Wenn diese Wärmefreigabe oder die Strömung sich periodisch ändern, kann dies zu periodischen Druckschwankungen führen. Für den Fall dass die Frequenz der Druckschwankungen einer Eigenfrequenz der Brennkammer (Raummoden) entspricht, kommt es zu stehenden, umlaufenden oder gemischten Moden in der Brennkammer. Es gilt die Entstehung dieser Moden besser zu verstehen, um Gegenmassnahmen ergreifen zu können, denn sie stellen eine die Lebensdauer herabsetzende Belastung der Brennkammer da. Diese Verbrennungsinstabilitäten sind charakteristisch für die heute gängige Bauform der Ringbrennkammer.

Die folgende Arbeit setzt sich aus experimenteller Arbeit, analytischen Methoden und Programmierarbeiten zusammen. Es werden mehrere Lautsprecher angesteuert um verschiedene akustische Moden anzuregen. Mithilfe von LabVIEW und MATLAB werden Schalldruckmessungen durchgeführt und daraus die Moden errechnet.

Rezente Forschung hat gezeigt, dass Verbrennungsinstabilitäten in Ringbrennkammern zu stehenden und umlaufenden azimuthalen Moden führen können. Das Verständnis dieser Moden ist derzeit noch unvollständig. Es ist das Ziel dieser Arbeit die Anregung von stehenden, umlaufenden und gemischten Moden in einer kalten, nicht durchströmten Brennkammer nachzuweisen. Dadurch sollen dieselben besser verstanden werden.

Die vorliegende Arbeit zeigt, dass eine begrenzte Kontrolle über das Schallfeld möglich ist. Während die Anregung von stehenden Wellen vergleichsweise einfach ist, konnten um-

laufende Wellen nur unvollständig generiert werden. Es ist allerdings anzumerken, dass die in dieser Arbeit angewandten Methoden vielversprechend sind, sofern sie weiter verfeinert werden.

Contents

1	Combustion noise and instabilities	1
1.1	Gas turbines and combustion noise	1
1.2	Combustion instabilities	3
1.3	Dominant mechanisms of combustion instabilities	6
1.4	Control of combustion instabilities	9
1.5	Wider framework of the work	11
2	Acoustics and pressure measurements	17
2.1	On pressure waves	17
2.2	Kundt's tube: the two microphone method	19
2.3	Numerical model in a Kundt's tube	23
2.4	Pressure measurements	26
3	Experimental setup	29
3.1	Setup description	29
3.2	Equipment	31
4	Data acquisition and procession	36
4.1	Data acquisition and analysis	36
4.2	MATLAB code for analysis	42
5	Results and discussion	45
5.1	Assumptions	45
5.2	Goal: standing, spinning and mixed modes	46
5.3	Microphone influence	49
5.4	Speaker influence	54
5.5	Eigenfrequency determination	56
5.6	Influence of the forcing amplitude	58

5.7	Amplitude variation between speakers	60
5.8	Influence of speaker position and phase angle	62
5.9	Influence of speaker position and phase angle 2	64
5.10	Influence of geometry	66
6	Conclusion	70
6.1	What do we know?	70
6.2	What could be done next?	70
	Appendices	78

Chapter 1

Combustion noise and instabilities

1.1 Gas turbines and combustion noise

A gas turbine usually consists of a compressor at the air inlet, a combustion chamber and a turbine as displayed in figure 1.1, whereas compressor and turbine are mechanically connected. The compressor located upstream increases the air pressure from atmospheric pressure and forwards the air to the combustion chamber. Fuel is added to the compressed air, then the mixture is ignited and the combusting gases become a high temperature flow. In order to use the energy stored in temperature and pressure the turbine transforms it into mechanical energy and feeds the compressor upstream. At the exhaust, a high speed gas flow leaves the turbine, which can be used for propulsion according to Newton's third law [17] .

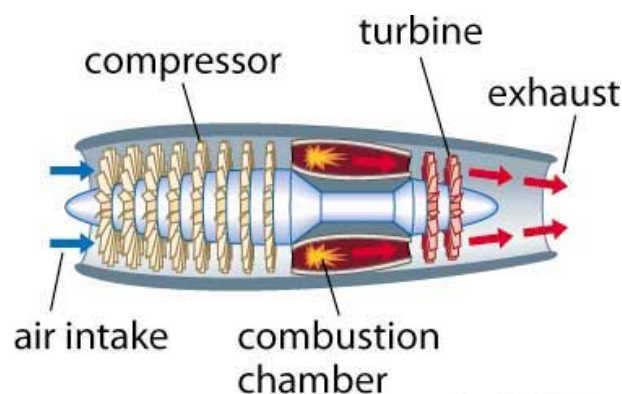


Figure 1.1: Scheme gas turbine [21]

Modern turbines are often designed using an annular architecture. The nozzles are distribut-

ed evenly around an annulus. This allows to build a compact and relatively light turbine.[9] Low weight and high power make the annular gas turbine the aviation industry's favorite. As will be shown in section 1.2, this comes at a price.

Turbines are run at high temperatures, providing higher power at lower weight than e.g. piston engines. As current materials are unable to cope with such high temperatures (at turbine inlet the temperature can still be over 1473 K [17]), gas turbines are built in a way that the flames do not touch the structure directly [9, 16].

The flow in the combustion chamber is complex as ignition of entering gas and re-ignition of circulating gas coexist [14]. If the circulating gas is additionally perturbed by the coupling of pressure waves and the combustion process, the unfavorable event of combustion instability occurs.

Combustion noise: a general problem

Combustion noise can be divided into direct and indirect noise. Direct combustion noise “is generated solely by the combustion process itself” whereas indirect combustion noise “is produced by the flow of hot combustion products through the turbine and exhaust nozzle” [9]. Apart from the problems arising with combustion instabilities (to be outlined below), there is a need to reduce engine noise. Both the need for lower emissions of noxious chemicals (mostly NO_x) and the increased awareness of noise pollution are a result of a change in mentality. As will be discussed later, noise and air pollution cannot be separated.

Gas turbines typically emit noise at frequencies between 100 and 2000 Hz, peaking between 300 and 500 Hz, independent of size, power or flame temperature [9]. In this context, only frequencies coinciding with natural frequencies of the combustion chamber are of interest, because only these lead to combustion instabilities.

It is, however, interesting to look at some parameters related to combustion noise [9]:

- radiated sound power
- thermoacoustic efficiency = $\frac{\text{radiated sound power}}{\text{heat released}}$

These two parameters are useful to describe combustion noise emission. In terms of estimation of combustion noise, however, one factor has proven to be most influential: engine power [9]. As engine power is closely related to mass flow rate and temperature level, it takes into consideration the influence of both upon combustion noise. As the core noise prediction is not the main topic of this thesis, the reader is referred to the works [9, 16] for further information on combustion noise.

1.2 Combustion instabilities

The easiest way to describe combustion instabilities is as interaction of the sound field and the combustion process in a volume. Whenever the flame becomes unstable (e.g. as it can be observed for a candle exposed to an air flow), the heat release fluctuates. The causes of this instability can be various, but the result is the same: since the heat release oscillates, the expansion of the heated gas oscillates too. These oscillations expand into the combustion chamber as sound waves. If the frequency of oscillation corresponds to a characteristic length of the combustion chamber or a multiple of this length, then the system becomes self-excited. The pressure influences flame dynamics and vice versa. This coupling phenomenon is called combustion instability and can be a serious problem. More information about eigenfrequencies and modes can be found in section 2. For the example of a candle in an air current, the energy is too low and the room usually too large for the described effect to be observed. A bunsen burner flame however, put into a tube of matching length and diameter can start “singing” [14, 16]. The system emits a tone related to its geometry when exposed to the burner’s flame. This only works if the burner and the tube are “matching”, just like a tuning fork is tuned to a particular tone.

Why study thermoacoustic instabilities?

Gas turbines today are mostly build according to annular architecture, as displayed in figure 1.2.

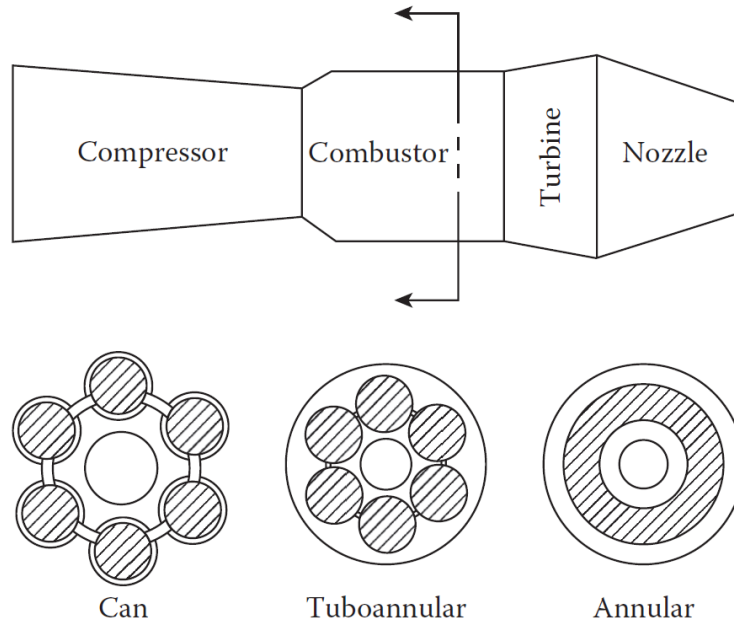


Figure 1.2: Gas turbine architecture [9]

This means that there are equidistant nozzles around an annular combustion chamber that are not separated through can dividers.

The demand for lower emissions has forced the industry to operate gas turbines with more air than needed. With the trend to shift to lower fuel-air ratios, as realized e.g. in diesel engines, the problem of combustion instabilities has gained in importance [9]. The fuel-air equivalence ratio (ϕ) is defined as the ratio of fuel to air relative to the stoichiometric ratio and describes how lean the mix is. The air-fuel equivalence ratio (λ) is its inverse:

$$\phi = \frac{1}{\lambda}$$

lean combustion for $\phi < 1$

As it turns out operation under lean conditions makes the turbines more predisposed to

combustion instabilities [14]. Together with the reduced size of the annular architecture, the trends have shifted the critical eigenfrequencies of the chambers into a band of typical combustion oscillation frequencies [6].

“Annular combustion chambers are commonly used in aircraft gas turbines because they fit efficiently between the axial compressor and the turbine. Their circumference is much longer than their length and width, so thermoacoustic oscillations tend to develop in the azimuthal direction.” [6]

That is why combustion instabilities have become a central issue of concern in the development of modern gas turbines. Additionally, damping in lean premixed turbines is lower as there are no liner holes and no wall cooling slots [2]. The excess of air in the combustion region has lowered the temperatures. More air is directed towards the combustion zone, resulting in less cooling air near the walls than in traditional chambers. This decreases the damping effect that the cold air had provided [14].

The critical eigenfrequencies are also referred to as the combustors natural frequencies. They are dependent on its geometry and the combustion temperature. There are longitudinal (along its flow axis), radial and circumferential (or azimuthal) modes. The modes are the shapes of the oscillation. Each mode corresponds to a natural frequency. As explained above, the circumferential modes are of primary interest. The lower circumferential modes are more interesting for two reasons: lower modes are more important in amplitude and higher modes are damped by viscous effects more strongly [16], causing less problems.

Low frequency combustion noise (50 - 180 Hz) is often referred to as rumbling or growling, whereas higher frequency combustion noise (200 - 500 Hz) is known as howling or humming [9]. While growling seems to go along more with aerodynamics and occurs at lower engine speeds (e.g. during start-up), howling seems to be the result of fuel pressure perturbations. The sources of combustion instabilities are discussed in detail in section 1.3.

In short: whenever a frequency of high amplitude combustion noise is near a eigenfrequency of the combustor, the acoustics and combustion might couple. By the same mechanism energy might be added with each cycle if heat release and acoustic field are in phase, it

could also be removed from the system if they are out of phase. This is described by the Rayleigh criterion [13, 14] for combustion.

The problem is that typically, gas turbines showing combustion instabilities within their normal operation range cannot be operated permanently. The flames might touch the wall and destroy them within seconds. Combustion instabilities “may cause structural damage, either because the resulting flow perturbations enhance the heat transfer or through vibration.” [1]

The redesign of gas turbines is often necessary at a late stage and happens at a high cost [9]. The boundary conditions such as upstream compressor and downstream turbine as well as the casing change the combustors natural frequencies [14]. Only as the combustor is mounted into the engine, combustion instabilities can occur, but don’t have to. A combustor might be perfectly stable when run outside the engine and yet show instabilities when mounted into it. As pointed out, low damping is characteristic of annular architecture, since there are few absorbing parts.

The influence of casing, compressor and turbine complicates predictions. Several attempts to model combustion instabilities have failed. One has to accept that reliable prediction of problematic combustion instabilities is impossible with the current understanding [9, 16].

1.3 Dominant mechanisms of combustion instabilities

Whether a gas turbine will show combustion instabilities or not can depend on its natural frequencies, influenced by its geometry and boundary conditions [14]. That is the influence of the combustor’s physical properties. The excitation is the counterpart. If both match, problems arise:

$$f_{eigen} = f_{excitation}$$

Since every combustion has several natural frequencies, every change in excitation might lead to coupling with a neighboring natural frequency.

The mechanisms leading to excitation are described in [9, 14] and are roughly divided into the four categories:

- fluctuations in the air supply to the combustor
- aerodynamic disturbances in the combustor
- variations in the fuel supply
- maldistribution of fuel in the combustion zone (leading to cyclic extinction and reignition)

An extensive overview over particular causes of combustion instabilities has been given in [9, 14] and is summarized below.

Fuel type

An interesting perspective for understanding the complexity of the problem is the characteristic combustion time. The inverse of the characteristic time is the eigenfrequency of the combustor. The characteristic time is the sum of the times for mixing, evaporation and reaction of fuel and air.

$$t_{combustion} = t_{mixing} + t_{evaporation} + t_{reaction}$$

It illustrates that the same combustor run with another fuel might act completely differently and that liquid fuel will behave differently than gaseous fuel, as it does not need time and energy to evaporate.

“The system becomes prone to instabilities when the overall combustion time becomes equal to a characteristic acoustic time of the combustor.” [9]

Tests have confirmed the theoretic insight that acoustic behavior is fuel dependent.

Operating conditions

As investigations have shown, the inlet temperature is important too. A higher inlet temperature reduces the characteristic time of reaction, as reactions occur faster at higher temperatures, which means it detunes the sound of the combustion. By this effect a drift of instability regions has been observed. All this is however difficult to predict and it is good to keep in mind that “any change in the characteristic combustion time could possibly move the combustor from a stable to an unstable region, and vice versa.” [9]

Ambient conditions

Experiments have also shown that both ambient temperature and humidity influence combustion pressure oscillations. This is important with regard to geographical differences.

Aerodynamic instabilities

On a more general note, a combustor needs to be stable (to a certain degree) by itself. As there is a complex airflow (recirculating air) within the combustor, ignition, cessation of combustion and reignition occur. That is another periodic mechanism that could couple with the combustors’ acoustic field.

Fuel-injection instabilities

Pressure pulsations in the fuel-injection system are maybe one of the more obvious causes. They lead to pulsations in heat release, such as coupling might occur. Additionally, the pressure in the fuel injection system determines spray characteristics e.g. drop size, distribution and spray angle and affects the heat release rate in a second way. The author of [9] specifically reminds the reader that fuel delivery might be a cause for combustion instabilities as well as a tool against them. Some examples of control measures, such as e.g. fuel delivery control, will be given in section 1.4.

Compressor induced oscillations

Pressure fluctuations do not necessarily have to issue the combustion process. Perturbations might as well be introduced by the air supply and come from the compressor upstream. This can be the case especially under conditions the turbine was not primarily designed for, such as start-up.

1.4 Control of combustion instabilities

Sustained combustion oscillations are the result of a feedback loop between the combustors acoustics and the heat release rate issuing combustion. The coupling mechanism is illustrated in figure 1.3.

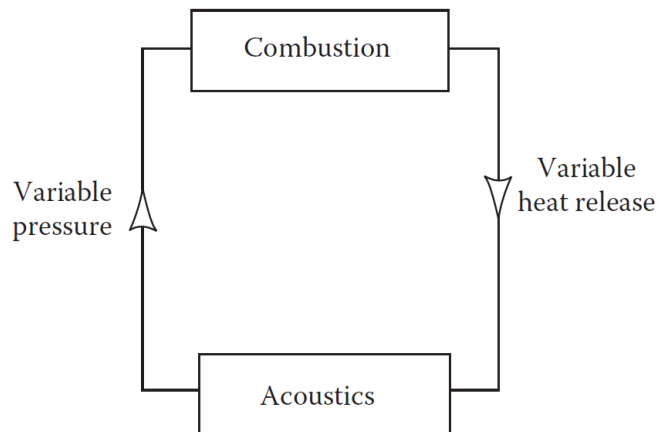


Figure 1.3: Coupling of acoustics and combustion [9]

Just like in most acoustic related topics, there are passive and active control methods.

Passive control

The chapter on combustion noise in [9] states that passive control techniques “have been widely used in industrial burners”. Control can be achieved by changes of the source of

fluctuations (e.g. fuel injector) or by increasing the damping of the system. These control measures are, like most acoustic measures, less effective at low frequencies and can include baffles, resonators or acoustic liners [9, 14]. Considering the space issue, which is often related to annular combustors and the fact that passive measures have to be tested step by step, it seems worth looking into active measures.

Active control

Active control of a dynamic system can be achieved by open-loop or closed-loop systems. While open-loop systems only take into consideration the current input and the model of the system, closed-loop systems are additionally equipped with a feedback loop. This means that open-loop systems can only react to an input with a prescribed general action. Whether the output reacts according to the model cannot be verified by an open loop system. Generally, open-loop control systems are less prone to control instabilities. The disadvantage is that they require a precise calibration, leaving closed-loop systems as the option generally preferred [9]. As closed-loop control systems monitor both input and output of a combustor, the adjustments to be made to the input can be more precise, taking into account the combustors reaction to previous inputs. A pressure sensor or flame detector downstream monitors the output by producing a signal varying in time. That signal is processed to adapt the input accordingly. The actuators typically used in combustion instabilities control systems are “acoustic drivers, flow valves with rotating or oscillating elements to produce periodic flaws, and shaking devices to produce mechanical oscillations.” [9]

Another method of intervention is the fuel staging technique. Explored in [14] it “allows the variation of the geometric position of the fuel injection”, hereby permitting to influence the heat release rate.

Examples of tested active control systems demonstrate how many ways there are to approach the problem, and that active control can be quite effective.

The typical measures aim at eliminating the oscillations by varying one of the inputs (air, fuel) or by adding a new input (spark, acoustic wave) in a manner that reduces the oscil-

lations. Some examples of active control are:

- pressure wave excitation
- pulsed gas jets in recirculating zone
- fuel injection
- inlet flow area variation
- preignition of some share of the fuel

Interestingly, the control measure does not necessarily have to occur at the frequency of the oscillation to be removed. Experiments showed that with active control over a wide frequency range (100 – 1000 Hz) a 160 Hz oscillation could be reduced [9]. Some other works show that even low and very low frequency (2 Hz) modulation can reduce the combustion oscillation.

“These results are interesting because they do not conform to the generally held view that fluctuations in heat release can only be smoothed out by repeated perturbations that occur at about the same frequency as the fluctuations.” [9]

1.5 Wider framework of the work

“The nature of azimuthal modes in annular chambers is still an open question.” [1]

It has been noted in [13, 19, 20] that a running combustion chamber does not stick to a certain oscillation mode, but shows continuous transitions between standing and spinning modes. These modes can be modeled by two waves with amplitudes A and B travelling in opposite directions around the annulus. If the spin ratio is defined in a similar way as the standing wave ratio [11], the modes can be described as standing, clockwise (CW) spinning or anti-clockwise (ACW) spinning [20].

$$SR = \frac{|A| - |B|}{|A| + |B|}$$

- $SR = 1$: ACW spinning mode
- $SR = 0$: standing mode
- $SR = -1$: CW spinning mode

A standing mode is an oscillation. This means that there are so called nodes, points where the pressure fluctuation is always equal to zero. Standing modes in an annular chamber occur if the waves travelling in opposite directions around the annulus have the same frequency and amplitude ($A = B$). Spinning modes occur if A or B is equal to zero.

If the waves “travel in a clockwise or anticlockwise direction, with the pressure and velocity nodes travelling at the speed of sound, they are called spinning modes. If the nodes are fixed in space and the wave modulates its amplitude without travelling, then they are called standing modes.” [6]

The mode can be called mixed if neither of the previous situations apply, meaning if A and B are both nonzero but not equal.

The simplification of a 1D plane wave in an annular chamber can, of course, not perfectly represent the 3D sound field that will really appear. If we consider the source of the oscillation a moving “hot spot” [10], meaning a local temperature maximum, the existence of several hot spots complicates the matter. As these hot spots rotate around the chamber, so does the acoustic field. It has been noted that not only one but several hot spots make an appearance in simulations [8]. This is mentioned to illustrate the complexity of the phenomenon.

The modal dynamics of self-excited azimuthal instabilities in annular chambers were investigated experimentally in [19]. The relation between time-varying pressure amplitude and global heat release was explored with the two microphone technique and chemiluminescence. To discover trends, the flame spacing was varied, with 12, 15 and 18 flames equally spaced, depending on the configuration. Further, the experiments were conducted with identical and alternating swirl (neighboring swirls in opposite directions). This is referred to as swirl configuration [19]. Finally, the fuel-air equivalence ratio ϕ was varied too, while staying in the lean range ($\phi < 1$).

The instabilities are described as the sum of waves travelling in opposite directions, just as in the present work. As the combustion oscillation is not stable, the amplitudes A and B vary over time. The results suggest that there is a “statistical prevalence for either standing or spinning modes (CW or ACW) depending on flame spacing equivalence ratio and swirl configuration.” Figure 1.4 illustrates this statistical prevalence, whose explanation would go beyond the scope of this work. As can be seen, the probability density is not highest (darkest) on the $A_+ = A_-$ line, but slightly offset. A_+ and A_- correspond to A and B in the current work.

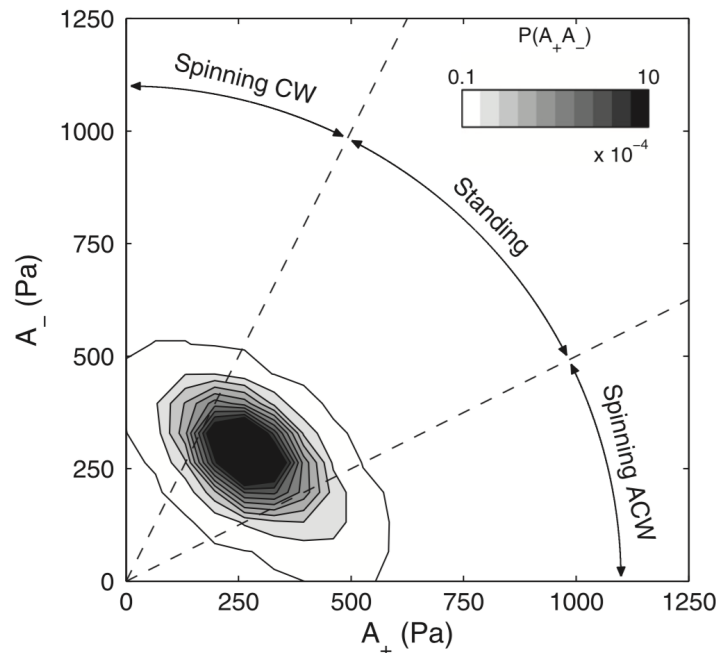


Figure 1.4: Statistical prevalence illustrated [19]

It is not yet clear why there is a switching between standing and spinning modes. Mostly, the modes described are neither purely spinning nor standing but mixed forms. If several modes share a frequency but have different mode shapes, they are called “degenerate modes”. The appearance of degenerate modes has also been described in other works [1, 8].

A theoretical study [6] suggests that noise might cause the modes to switch between standing and spinning modes. As combustion noise is partly random, meaning present at various frequencies, this hypothesis seems plausible, but it does not match to the statistical preva-

lence (despite symmetry) described in [19]. According to that theoretical study there is a preference for spinning modes in the case of lower transverse velocity forcing. For higher transverse forcing it suggests standing waves to be the only stable state.

“In summary, current thermoacoustic models cannot explain why standing modes in symmetric annular chambers should be a preferred state of the system, despite experimental evidence that they sometimes are.” [6]

The author of [6] also suggest that “transversal (velocity) forcing plays an important role in annular combustion instabilities, and should be taken into account to accurately predict instabilities in annular configurations. ” The disadvantage of transversal forcing is that it breaks the symmetry.

To avoid this, the authors of [20] applied acoustic forcing onto the chamber’s acoustic field. The set up is an operating combustion chamber which is excited using two loudspeakers opposite to one another as can be seen in figure 1.5. The signal to the speakers is identical except for the phase which is 180° . A standing mode is excited this way.

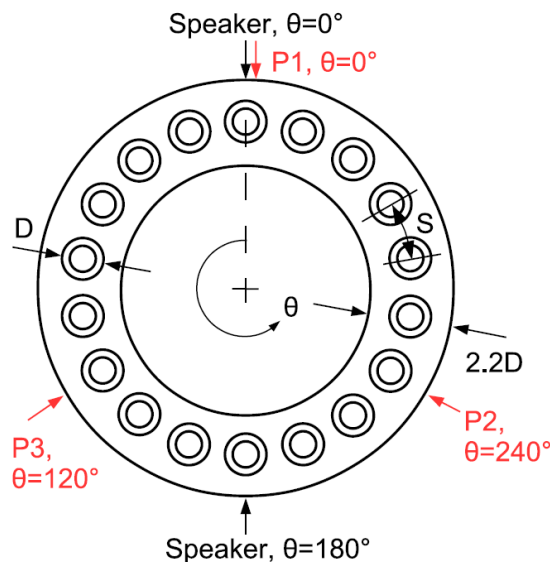


Figure 1.5: Annular chamber with acoustic drivers as used in [20]

It has been shown by the authors that large circumferential modes can not only be excited,

but also controlled in frequency, amplitude and orientation. In a best-case-scenario, the spin ratio of a wave could totally be controlled, permitting to excite ACW and CW spinning waves, standing waves and any form of mixed waves (controlling A and B perfectly). However, close to the natural frequency, the imposed oscillations' energy seems to drift into the self-excited (flame issued) state. The result is a mixed mode. This means the control over the self-excited state is limited if the two opposite speakers are in anti-phase (180°).

Useful for this work is the following information: the measured amplitudes increase with acoustic excitation compared to oscillations induced by flames only, demonstrating the possibility to actively modify the acoustic field issuing flames [20]. That result is a motivation to explore the modal dynamics further.

As seen, two opposite speakers in anti-phase and run at an eigenfrequency, will lead to a standing wave due to the combustors' symmetry. Spinning waves cannot be created with this configuration. The introduction of several speakers at different physical angles and with different phase shifts might solve this problem and will be tested in the current work. Figure 1.6 shows the setup used. Each speaker has to be controlled individually to realize other phase shifts than just anti-phase. Controlling the sound field in an annular chamber, just by the means of acoustic drivers, is the aim of this work. The superposition of the two standing waves could lead to a spinning or mixed wave. The goal is to gain better understanding of the modal dynamics of annular chambers and the possibilities of acoustic forcing. The importance of forcing amplitude, phase shift, speaker position and number is to be investigated.

A lot of research has already been done in that field and the nature of these oscillations might lay within the acoustic properties of the combustion chambers. A short introduction into the theory of acoustics will be given before the experimental setup is described.

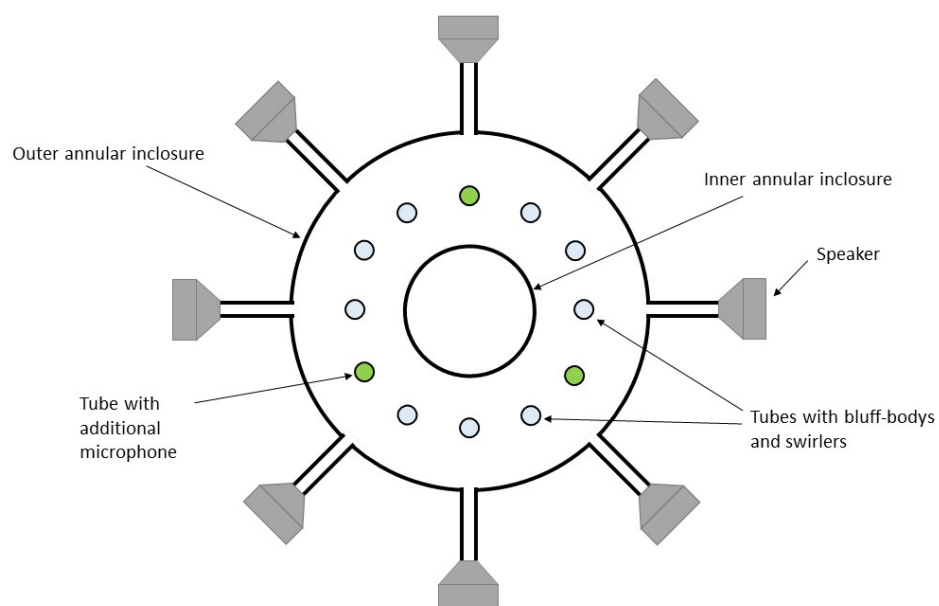


Figure 1.6: Annular chamber equipped several acoustic drivers, permitting to influence the spin ratio by shifting the phase between the signals of the drivers

Chapter 2

Acoustics and pressure measurements

2.1 On pressure waves

For the understanding of thermoacoustic instabilities in gas turbines, a basic understanding of both gas turbines and pressure waves is required. Pressure waves are longitudinal waves, which means the oscillation occurs in the same direction as the propagation. They propagate with the speed of sound c , which is a function of air temperature [11]. The influence of temperature is important and remarkable: the speed of sound c at 293 K is around half of c at combustion temperatures e.g. 1473 K.

$$c(T) = \sqrt{\frac{\kappa R}{M_{mol} T_0}} \text{ with } T_0 \text{ in (K)}$$

(κ , R and M_{mol} explained in [11])

$$c(293K) = 343 \left(\frac{m}{s}\right)$$

$$c(1473K) = 770 \left(\frac{m}{s}\right)$$

As mentioned earlier, the eigenfrequencies of the combustion chamber are of interest in this work. They can be approximated using the formula for the n -th circumferential (or azimuthal) eigenfrequency of a combustion chamber [15, 18]:

$$f_n = \frac{n \cdot c_{mean}}{C_{mean}}$$

With C_{mean} being the mean circumference of the annular chamber, the formula admits that the wavelength for $n = 1$ is equal to C_{mean} . It is clear that the eigenfrequency is proportional to c . Figure 2.1 illustrates why the formula is an approximation only. It shows the spacial distribution of the heat release rate, leading to temperature fluctuations. The differences in sound speed around the annulus are a result of differences in temperature. The mean sound speed might not very well represent the variation of sound speed around the annulus, in such a complex temperature field. The formula for the eigenfrequency is also an approximation only, because a 1D sound field is assumed, ignoring reflections and propagation towards outside the chamber (more on 1D assumptions in section 5.1).

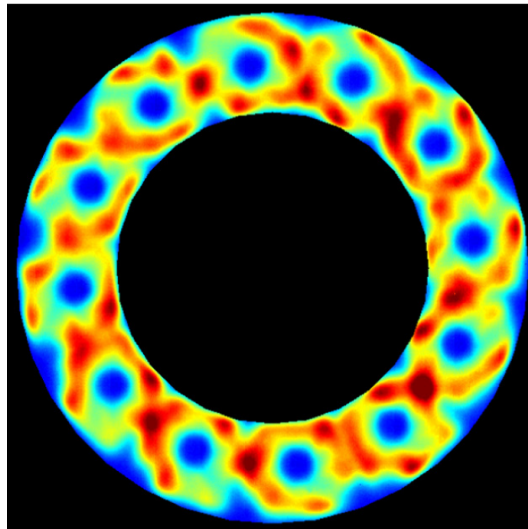


Figure 2.1: Spacial heat release distribution in an annular combustion chamber [19]

In order to better understand the role of pressure waves in the formation of combustion instabilities, we will take a look at the 1D wave equation [11] and its solution:

$$\frac{1}{c^2} \frac{\partial^2 p}{\partial t^2} = \frac{\partial^2 p}{\partial x^2}$$

The solutions by d'Alembert [11] can be written as follows, representing two monochromatic pressure waves travelling into opposite directions:

$$p(x, t) = (Ae^{-j\omega x} + Be^{j\omega x})e^{-j(\omega t - \phi)}$$

with

$$k = \frac{\omega}{c} = \frac{2\pi}{\lambda} \text{ (m}^{-1}\text{)}$$

$$\lambda = \frac{c}{f} \text{ (m)}$$

$$f = \frac{1}{T} \text{ (Hz)}$$

$$\omega = 2\pi f \text{ (Hz)}$$

$$\phi \text{ (rad)}$$

The wave number k describes the number of oscillations per length, λ , the wavelength, being the length the sound propagates in one period T , f being the frequency of oscillation. The angular frequency ω describes the angle covered in one second and ϕ the phase angle.

Modes are standing waves that can be described by a decomposition into two waves of same frequency, amplitude and matching phase, travelling in opposite directions: Figure 2.2 shows the spacial pressure distribution of a standing wave for various times. As can be seen, there are locations where the amplitude is always equal to zero, called nodes.

The next sections illustrate the connection between standing modes in a duct and in an annular combustion chamber. The two microphone is illustrated for both cases.

2.2 Kundt's tube: the two microphone method

Figure 2.3 shows a speaker in a tube. If we admit a plane wave to travel from $x = 0$ along the duct and be reflected at the rigid end, the result is two waves travelling in opposite directions. The amplitude B is determined by the amplitude A and the reflection factor of the end of the tube.

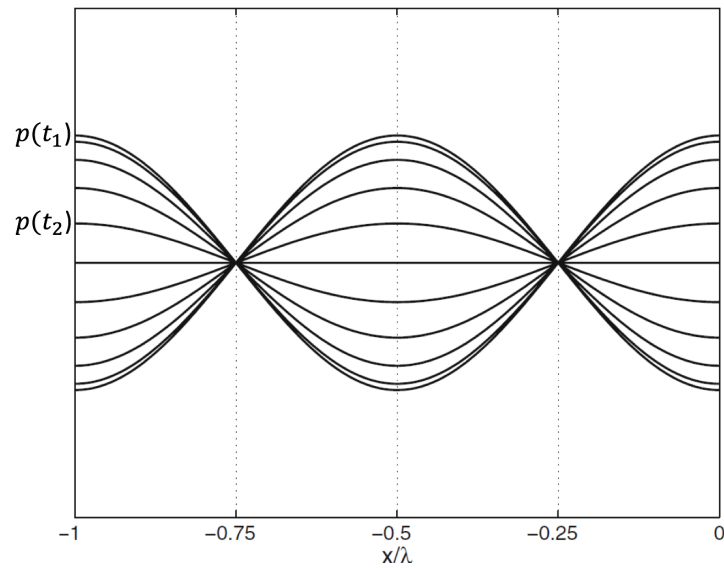


Figure 2.2: Standing wave pressure distribution for various times [11]

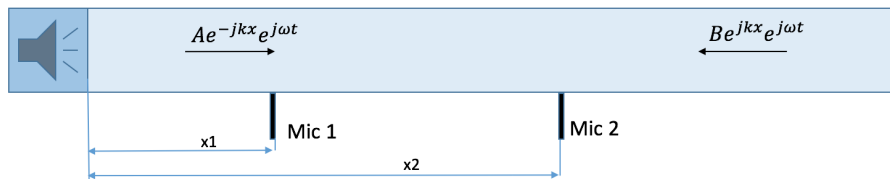


Figure 2.3: Kundt's tube with reflecting end

This setup is e.g. used to determine the absorption coefficient α of a material placed at the end of the tube [12]. If A and B are known, α can be determined. To find A and B the two microphone method is applied. As a matter of fact only two microphones are necessary to determine A and B . If the positions x_i of the microphones are known and the time pressure series measured, A and B are found using the wave equation's solution. To simplify, as in [12], Δx represent the distance between the microphones. The equations are valid for all times t .

$$p(x_1) = p_1 = Ae^{-jkx_1} + Be^{jkx_1}$$

$$p(x_2) = p_2 = Ae^{-jkx_2} + Be^{jkx_2}$$

This system of equations is solved for A and B:

$$A = \frac{p_2 - p_1 e^{jk\Delta x}}{e^{-jk\Delta x} - e^{jk\Delta x}}$$

$$B = -\frac{p_2 - p_1 e^{-jk\Delta x}}{e^{-jk\Delta x} - e^{jk\Delta x}}$$

The amplitude A and B can only be calculated assuming the pressure variations have a known frequency. That frequency is included in the wave number and required to determine A and B.

We can calculate the n-th circumferential eigenfrequency of a tube using the formula [11]:

$$f_n = \frac{n \cdot c_{mean}}{2L}$$

$$f_1 = \frac{c_{mean}}{2L}$$

$$\lambda = \frac{c}{f} = 2L$$

This means one wavelength of the first mode corresponds to twice the tube length. The first mode is the superposition of two travelling waves of same frequency and amplitude (assuming $A=B$ and a reflection factor of 1). The result of this is a standing wave, just like displayed earlier in figure 2.2.

If we replace the reflecting end by another speaker (figure 2.4) with the same input then the result is the same:

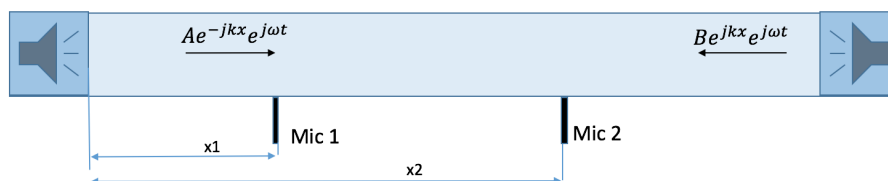


Figure 2.4: Kundt's tube and two acoustic drivers

As for now, only a standing wave has been demonstrated. If $A=B$ the wave is perfectly standing. If A or B is vanishing, then it is a purely travelling wave. If A and B are nonzero and not equal, it is a mixed waveform.

This is interesting if we imagine the tube to be bowed and the ends put together so it becomes an annulus (figure 2.5). The result is an approximation of our combustor. The yellow arrow marks the transition between the two models. The assumptions made for this transition are described in section 5.1.

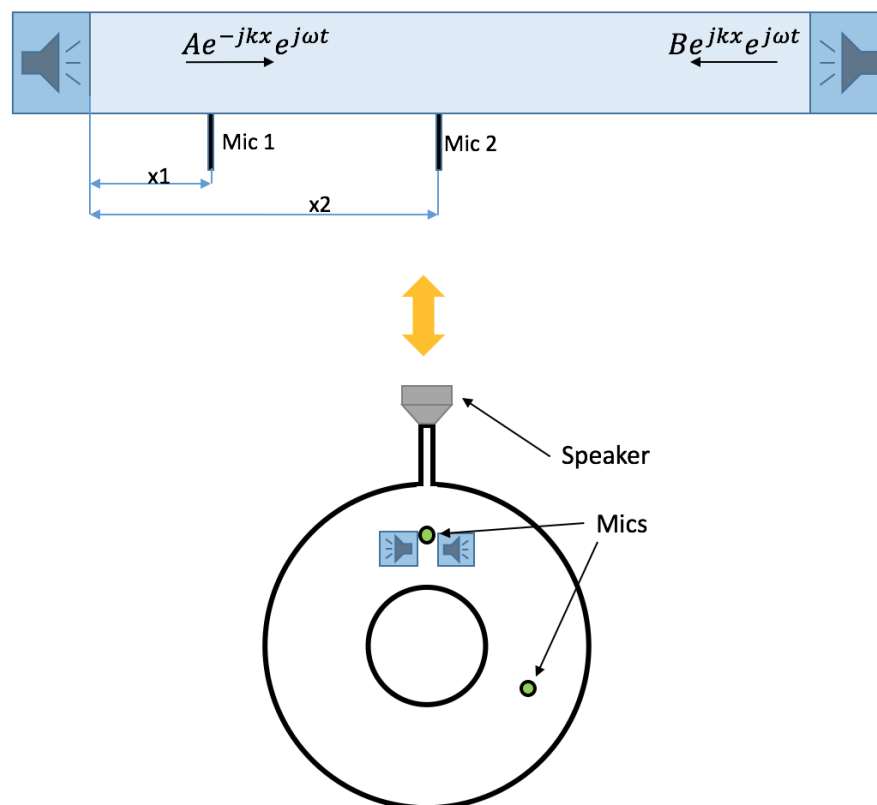


Figure 2.5: Analogy: the tube can be imagined as bowed, its ends connected. The result nearly is an annular chamber. The two microphone method can be applied in the same way as in the tube.

The wave coming from the speaker splits into two identical waves travelling through the combustor in opposite directions between inner annulus and outer annulus. In this case A

will always be equal to B, admitting perfect symmetry at an excitation frequency equal to the combustors eigenfrequency. The eigenfrequency in this case is double the eigenfrequency of the tube. Since there is no reflection at an end (its endless) the wavelength has to be equal to a full combustor circumference (analogy to the length of a tube). If this is the case, the wave fits perfectly into the combustor and when it has travelled around the annulus once, it gets reinforced by the speaker being in phase. Assuming no acoustic losses, the amplitudes of A and B will grow towards infinity. In this constellation standing waves can be excited by setting the speaker excitation frequency equal to the eigenfrequency. But due to symmetry $A = B$ will always be true for a perfectly manufactured combustor.

If it was possible to control A and B independently, mixed and spinning modes could be realized. This requires the introduction of (at least) one other speaker and a matching phase shift between the signals feeding the two speakers. This is discussed further in chapter 3 on the experimental setup.

2.3 Numerical model in a Kundt's tube

The MATLAB code corresponding to the following steps can found in the appendix 6.2.

To illustrate the two microphone method, a numerical simulation with MATLAB is done. After the command lines to close windows, clear command window and variables, frequency, speed of sound and wave number are defined. For the amplitudes of the waves travelling along the duct in opposite directions, any values can be chosen. It is these values that are to be reconstructed using the two microphone method. For purpose of recognition A is chosen to be 25 and B to be 15. The microphone positions can also be chosen. The microphones were labelled during previous experiments. The microphones' labelling (mic2, mic3) is being maintained instead of renaming them (1,2...), to ease comparing earlier works with the present work.

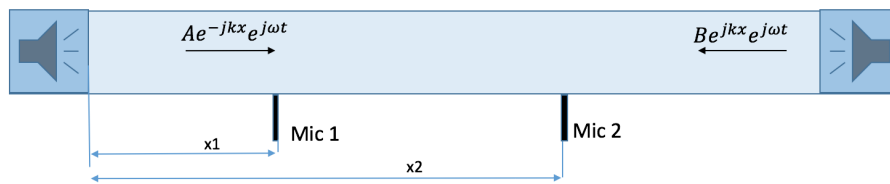
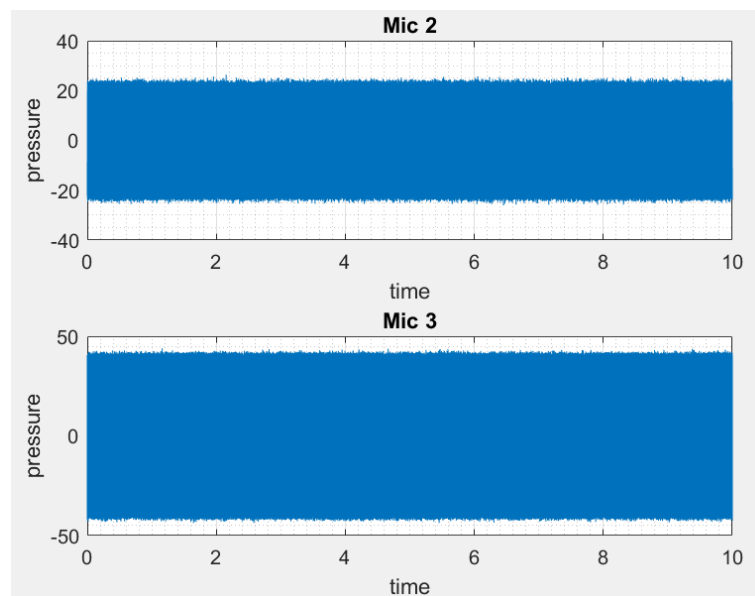


Figure 2.6: Kundt's tube with two acoustic drivers

A time vector is created, using timesteps defined by the sampling frequency. The sampling frequency is chosen to be 51200 Hz as it will later be used for the measurements. The measurement time and sampling frequency determine the total number of values N sampled. Using a function, the complex pressure values are collected for each position and all times defined in the t -vector.

Gaussian noise is added to the function values to simulate measurement noise. The function itself uses the solution of the wave equation (2.1) and can be found in the appendix 6.2.

The outputs of the function are complex time pressure values gathered in a vector. According to the time convention in [11], the real parts represent the pressure, as it would be measured by the microphones.

Figure 2.7: Pressure time series at both locations x_2 and x_3 including gaussian noise

The pressure time series is then FFT transformed and scaled as described in chapter 4.

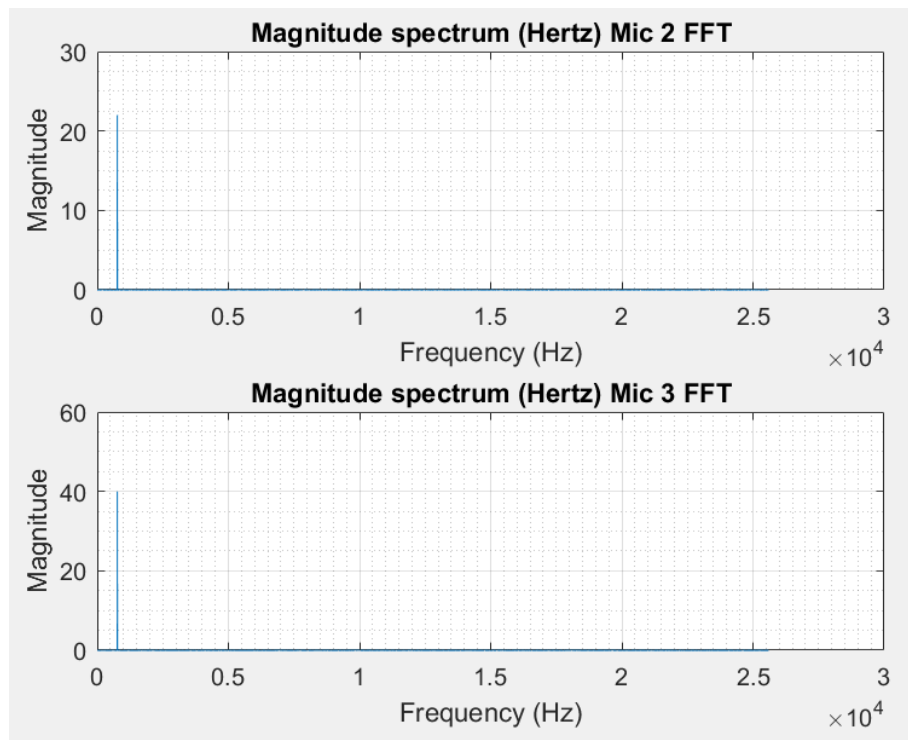
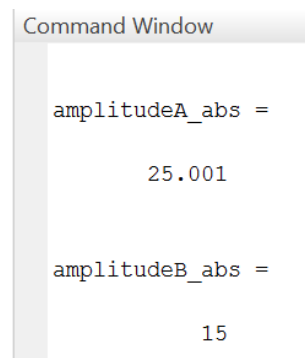


Figure 2.8: FFT of pressure time series

The maximum of the transformed series occurs at the excitation frequency (765 Hz). Its' complex magnitude displayed in figure 2.8 is used to apply the two microphone method.

The function returns the complex amplitudes A and B, which are close to the initial values. The absolute value corresponds to what was initially chosen for A and B. The small error comes from the noise, which was added to recreate more realistic simulation conditions.



```
Command Window

amplitudeA_abs =

    25.001

amplitudeB_abs =

    15
```

Figure 2.9: A and B determined using the two microphone method

2.4 Pressure measurements

The previous sections demonstrated how to reconstruct the sound field using two microphones. The normal procedure for pressure measurements is described. Several influences have to be taken into account [4, 5]:

- the type of microphone: free field condenser microphone
- wind/flow: consider a windscreen
- frequency range and sensitivity of the microphone
- reflections from objects around the microphone
- air temperature
- air humidity
- vibrations
- background noise
- include detailed report on measurements (including sketch, type and serial number of microphones, calibration method, background noise level, environmental conditions, data on object being measured, date and time)

The conditions in the room where the following measurements are done can be considered stable, facilitating the evaluation of the measurements. Temperature and humidity are assumed constant, as they are regulated by the building technology. The free field microphones are suitable for these experiments as the results are to be compared to one another, and every microphone has the same geometric boundaries. Figure 2.10 shows schematically how the microphones are placed in the tubes below the combustion chamber. A rubber ring between microphone and tapping seals the tube from the outside. The reflections are not an issue, as the geometry around the microphones is the same and the aim is comparison. The frequency range of the microphones is 4 Hz to 100 kHz, meaning beyond everything required for these experiments (typical combustion noise frequencies: 100 Hz to 2 kHz) . The amplitudes of vibration at the rig are expected to be very small, as the only source of excitation is the sound field, whose energy is low compared to the typical energy of mechanical vibrations.

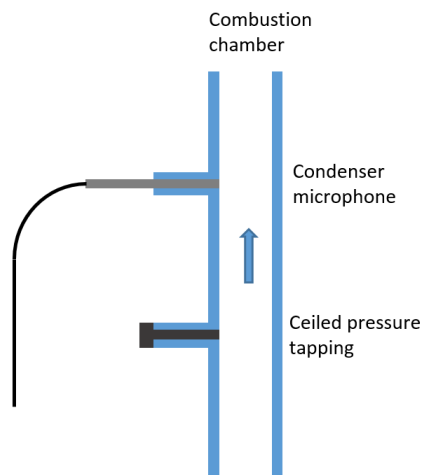


Figure 2.10: Microphone position in pressure tapping

Microphone calibration

The microphones used are described in section 3.2. With an uncertainty of 0.3 dB (95 percent confidence level) those microphones should be precise enough for the measurements

intended. Since the objective of the measurements conducted in this experiment is the reconstruction of the acoustic field by tendency (A and B are expected to change a lot), the last calibration dating back to less than 2 years prior to this work can be assumed to be enough. The long term stability according to the manual is 1dB/1000 years. However, to make sure the microphones are not damaged, their responses to the same input have been compared for different frequencies. The input is a sine tone created by the signal generator.

The results can be seen in table 2.1 and are discussed further in section 5.3:

Calibration microphones				Error rel. to mean amp			
Exc. frequency	Mic2 amp	Mic3 amp	Mic5 amp	Mean amp	Mic2 %	Mic3 %	Mic5 %
250	0.30559	0.30916	0.30428	0.30634333	-0.2459115	0.91944768	-0.6735362
500	0.31002	0.32014	0.30975	0.31330333	-1.0479727	2.18212382	-1.1341511
750	8.741	8.8132	8.7247	8.75963333	-0.2127182	0.61151722	-0.398799
760	10.126	10.253	10.107	10.162	-0.354261	0.89549301	-0.541232
1000	0.91695	0.94889	0.94951	0.93845	-2.2910118	1.11247269	1.17853908
1250	0.85143	0.87844	0.89155	0.87380667	-2.5608258	0.53024697	2.03057885
1500	3.2403	3.4479	3.2476	3.31193333	-2.1628857	4.10535639	-1.9424707
1750	1.4655	1.644	1.6771	1.59553333	-8.149835	3.03764676	5.11218819

Table 2.1: Microphone comparison and error: each microphone's error is calculated relative to the mean value of the three microphones for different frequencies

The values displayed in the tabel 2.1 are obtained by treatment of the time pressure series. Its trend (illustrated in figure 4.3) issuing the DAQ is removed. Then it is transformed using the DFT as explained in chapter 3. The maximal value of the DFT is of course the one at the excitation frequency (figure 4.4 in chapter 4). It is compared for all three microphones, which are placed at the exact same location in the combustor one after another.

As can be seen in the table, the difference between the microphones at the resonant frequency of roughly 760 Hz is under 1 percent. The microphones show little difference in response, except for higher frequencies, for which damping in the combustor is higher. This is not an issue for the current work as discussed further in 5.3, as the frequency of interest is the eigenfrequency, which shows little error.

Chapter 3

Experimental setup

3.1 Setup description

The experiments were conducted on the rig displayed in figure 3.1. It was conceptualized as a test combustion chamber and parts of it were used for the works [19] and [20].

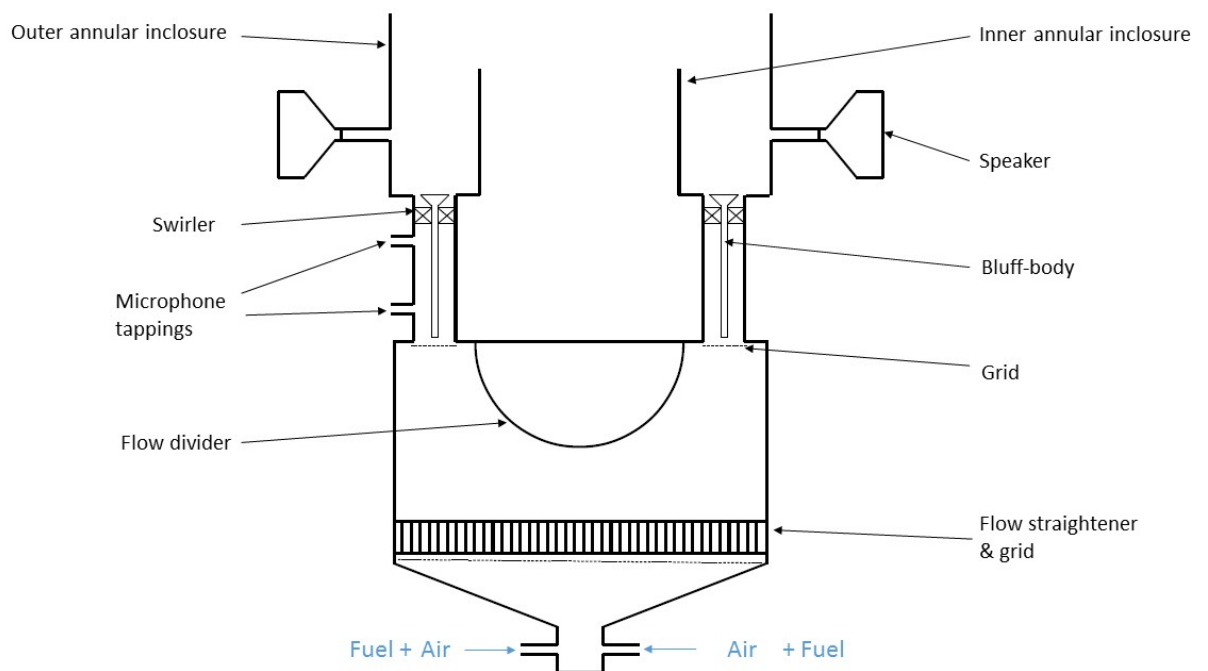


Figure 3.1: Experimental rig in sectional view as used for the current work. [19]

Compared to a typical gas turbine combustor, the number of flames (and tubes) is reduced. Hence the diameter for a typical combustion chamber is typically bigger, reducing the first

eigenfrequency. As the following experiments are run cold, c is much lower, compensating for the size difference and explaining why the eigenfrequency measured (760 Hz) is still near usual values (section 1.2).

The equipment used will be described in section 3.2. The actual rig is displayed in figure 3.4. Starting from the bottom the setup is the following: On the bottom is the air and supply connection. For these experiments neither fuel nor air are used. The experiments are run “cold” and without flow, as the characteristics of the annular chamber itself and the nature of the azimuthal modes are to be studied. More on hypotheses on this matter can be found in section 5.1.

Above the entry there is a flow straighter and a grid, followed by a flow divider. If there was a flow, it would be divided between the 12 tubes containing centered bluff-bodys and swirlers on the upper end of the tubes. The swirlers have a rough surface and make sure the flow is turbulent before the mix enters the combustion chamber. The microphones are attached to the pressure tappings on 3 of the 12 tubes. There is a 120° angle between neighboring microphones. The positioning of the microphones prior to the combustion chamber ensures the temperatures are within the microphones’ temperature range.

Around the rigs annular enclosure, eight speakers are mounted equidistantly such as 45° angles separate them (fig. 3.2).

In illustration 3.3 the general setup for acoustic experiments on the rig can be seen. The acoustic input into the system combustion chamber comes from a four channel frequency generator and gets amplified through an audio amplifier before it reaches the speakers. In the case of experiments with flow and/or combustion there would be a flow input entering the combustion chamber, regulated by flow meters and consequently flowing by the microphones into the chamber. The output of the system combustion chamber are the voltage values given by the microphones. These voltage time series are to be converted into pressure time series before they are processed as described in section 4.1.

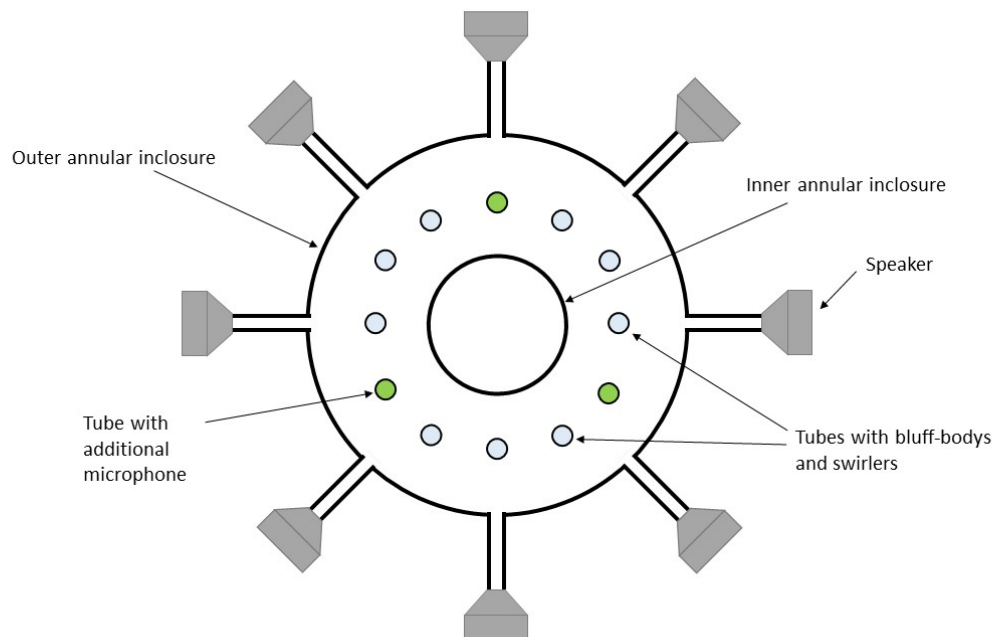


Figure 3.2: Speaker and microphone positions of the experimental rig in top view

3.2 Equipment

Rig

The rig used for the experiments is displayed in the figures 3.1, 3.2 and 3.4.

Frequency generator

The four channel frequency generator of the type “Aim TTi TGA1244” is used to generate the sinus voltage signals at adjustable frequencies and with adjustable relative phases.

Amplifiers

The signals coming from the frequency generator are amplified using amplifiers of the type “qtx PRO1000 Stereo Power”.

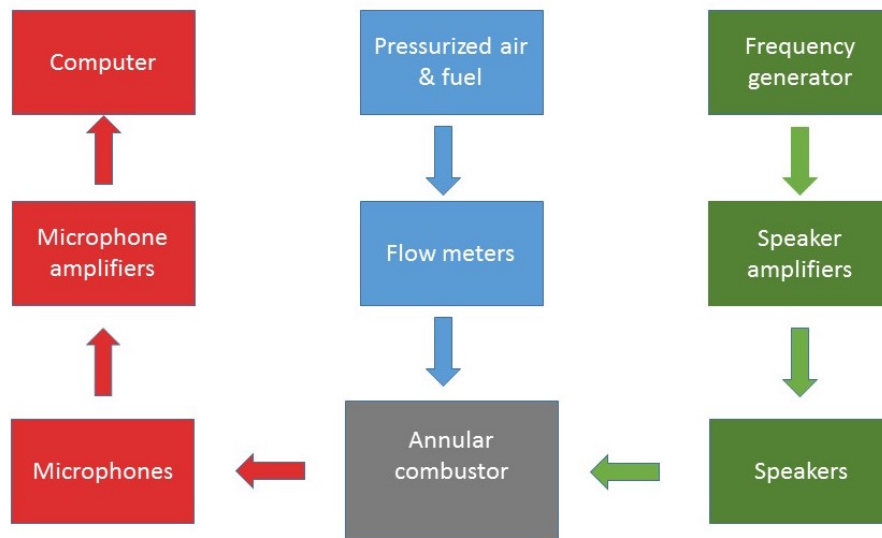


Figure 3.3: The experimental setup: inputs and outputs

Speakers

The acoustic drivers used to transform the electric energy into pressure waves are referred to as speaker in the current work. They are supposed to be identical and of the type “adastra HD 50 16 Ohm Driver Unit”.

Multimeter

A multimeter’s root mean square (RMS) function was used to verify the inputs at the different speakers and adjust the frequency generator so they become equal. This eliminates the influence of the amplifiers imprecise settings and avoids calibration.

Microphone units

The microphones units are composed of the actual microphone and an amplifier integrated in the microphone base. Each microphone was calibrated in combination with its amplifier. The last calibration dates back to less than two years previous to this work (July 2014). To check the microphones are not damaged, their response is compared in section 5.3.

The microphone unit type is Brüel and Kjær 4939-A-011 with an uncertainty of 0.3 dB.

- Microphone labelled 2: Unit Serial 2922006 Type 4939-A-011
Combined sensitivity=4.13 mV/Pa
- Microphone labelled 3: Unit Serial 2922007 Type 4939-A-011
Combined sensitivity=4.07 mV/Pa
- Microphone labelled 5: Unit Serial 2922003 Type 4939-A-011
Combined sensitivity=4.13 mV/Pa

DAQ

The analog signal coming from the microphones enters the type “DAQ NI 9215”, which is placed in the base “NI 9174”. Connected by USB to the computer, LabVIEW permits digitalizing the signal using the DAQ and controlling the sampling frequency and measurement time in the front panel (chapter 5).



Figure 3.4: Experimental rig

Chapter 4

Data acquisition and procession

4.1 Data acquisition and analysis

The data coming from the microphone amplifier is sampled by aid of a NI DAQ including an analog-to-digital converter. A LabVIEW program displayed in fig. 4.1 and 4.2 allows to control the number of values to be collected (N) and the sampling frequency (f_s), defining the measurement time: $\frac{N}{f_s}$. In order to get maximal resolution and considering the expected voltages with aid of the microphone sensitivity, the voltage range of data acquisition is chosen to be $\pm 1V$. The sampling frequency for the experiments is 51.2 kHz. The measurement time varies between five and ten seconds.

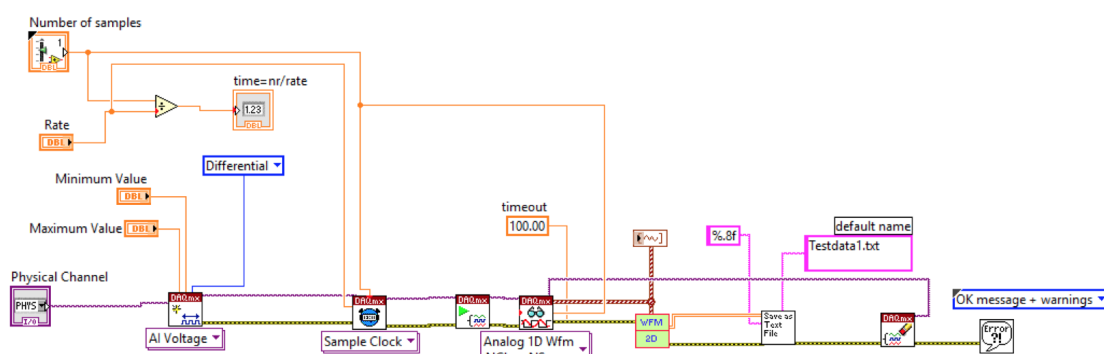


Figure 4.1: LabVIEW block diagram

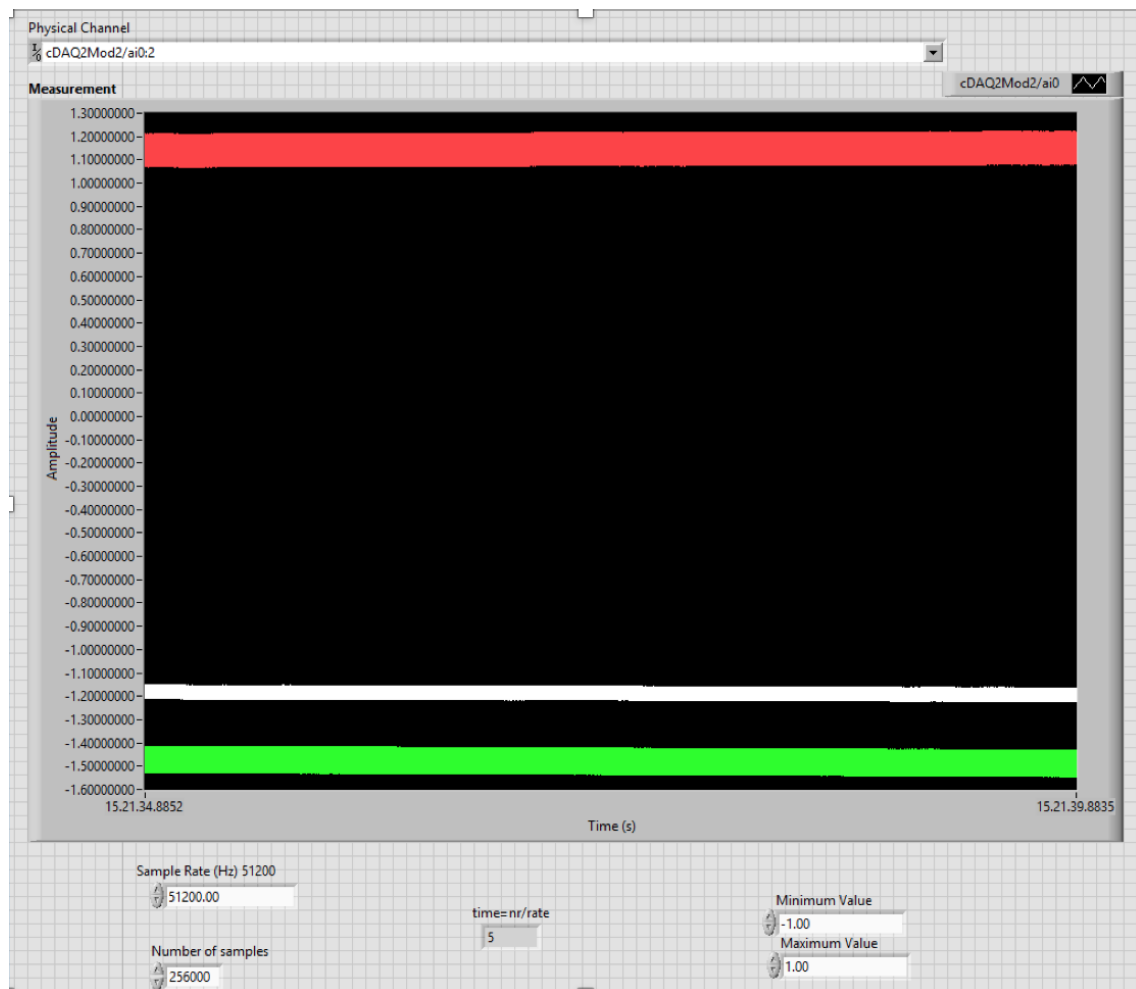


Figure 4.2: LabVIEW front panel

As the voltage acquired by the DAQ is not only dependent on the microphone's capacitor, the data has to be processed before it can be analyzed. There is not only an offset of the data, but a time varying offset, as can be seen in fig. 4.3. To eliminate this offset a moving average is used. The moving mean is usually used to smoothen a signal by eliminating the higher frequencies contained. In this case however, the moving mean value is subtracted from the signal. Figure 4.3 illustrates why this is necessary. This operation removes the changing offset and provides a signal oscillating around the zero-volt-line.

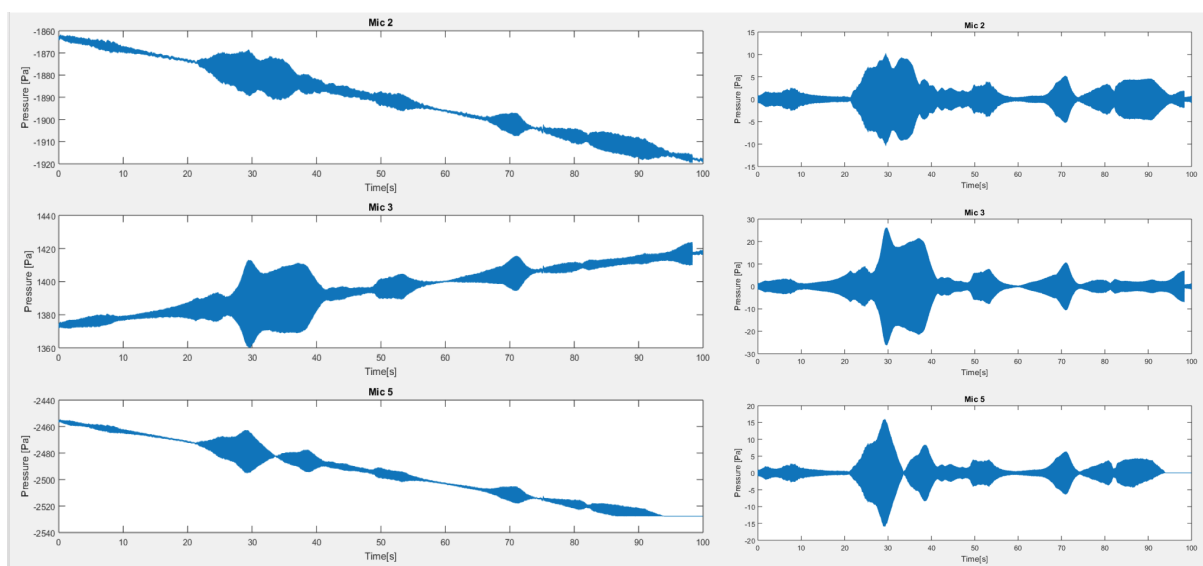


Figure 4.3: Detrending the signal (left) to eliminate the time-varying offset (right)

The sensitivity of the microphones is found in the calibration sheet and given in V/Pa. As the offset is removed, the voltage time series divided by the sensitivity returns the pressure (in Pa).

The pressure time series from the two microphones contains all the information required to investigate the modes occurring in the combustion chamber. One of the tools is the Fast Fourier Transform (often referred to as FFT). It allows to get the frequency spectrum by integration. The frequency spectrum contains the exact same information as the time series, but it allows a change of perspective, as it displays the importance of the various frequencies contained in the signal. In many cases the frequency spectrum allows identification of noise or vibration sources. In this case it allows to get a more exact amplitude. As the FFT requires an integration from minus to plus infinity and it is a discrete signal which comes from the data acquisition device DAQ, one is forced to use the discrete Fourier transform (DFT). The FFT is symmetric, which means that a transformation back and forth leads to the initial signal. But the DFT is calculated in non symmetrical way. This means the result is not mirrored at the y-axis but at the Nyquist frequency. The maximal detectable signal frequency is called Nyquist frequency and limited to half the sampling frequency. If there are higher frequencies contained in the signal, they are attributed to lower frequencies,

leading to an error [7]. As the Nyquist frequency is a lot higher than the highest frequency in the signal, such an error can be excluded.

$$f_{Nyquist} = \frac{f_s}{2} = f_{max.detectable}$$

The DFT definition is as follows:

$$x(n) = x(n \cdot \Delta t)$$

$$X(k) = \sum_{n=0}^{N-1} x(n)e^{-j2\pi k \frac{n}{N}}$$

The sum is actually two sums:

$$X(k) = \sum_{n=0}^{N-1} x(n)\cos(2\pi k \frac{n}{N}) - j \sum_{n=0}^{N-1} x(n)\sin(2\pi k \frac{n}{N})$$

$N = f_s t_{meas}$ is called the block size.

The definition used here is the same one MATLAB has implemented. The sum adds up the pressure of the signal for each bin, resulting in a pressure indicated by the DFT which is N times too high [3]. The result of the DFT is attached in a “mirrored” version at its end, so the pressure of the frequency peak is only half the real pressure. The other half is in its mirrored equivalent at the end (fig.4.4). Thus one has to multiply the result of the DFT by $2/N$.

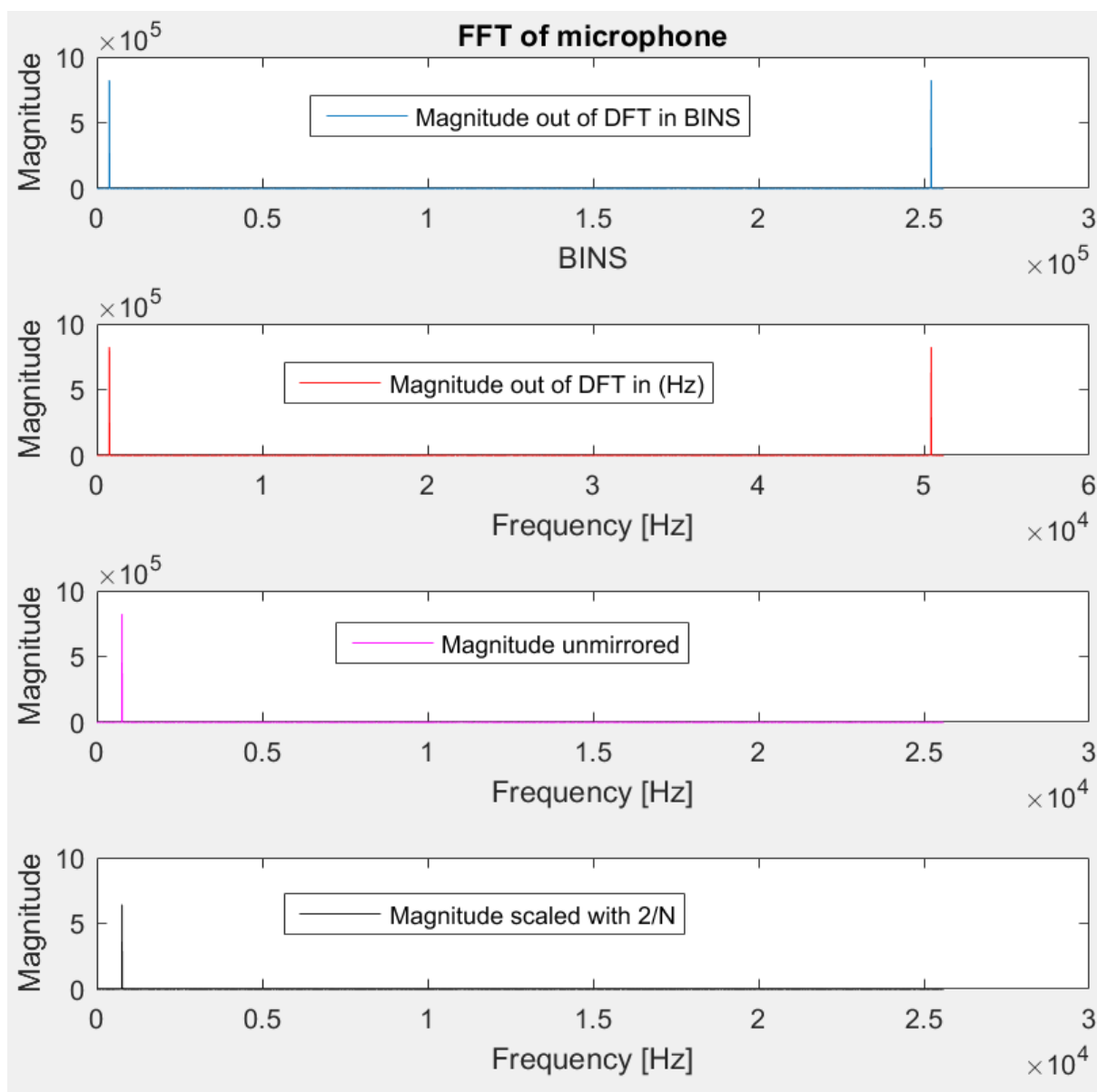


Figure 4.4: Stepwise treatment of the DFT signal: (top): DFT, (2nd): conversion to frequency, (3rd): unmirrored, (bottom): scaled

The mirrored version at its end issuing to symmetry for periodic and time-discrete signals can be ignored. Only the interval $[0 - N/2]$ of the frequency domain is of interest as illustrated in figure 4.4. The mirrored frequencies, attached for bin values greater $N/2$, do not provide any additional information (fig. 4.4). When the correct magnitude is of interest, as mentioned before, the DFT magnitude values have to be multiplied by $2/N$. The factor 2

compensates for leaving the mirrored frequencies' magnitudes as displayed in figure 4.4.

To get the amplitudes of both waves travelling in opposite directions, the complex magnitude of the signal at the frequency of interest is needed. So if the excitation occurs at 1000Hz we expect the FFT spectrum of the time pressure series to have a clear peak at 1000Hz. To automatize the peak finding, a peak detection function is used. It compares two following frequency values and gives out the magnitude values if the difference of the actual value and the previous value is bigger than Δ . The complex value found is put into the two microphone method's equation to get the amplitudes of the two waves.

For continuous signals, the DFT is only an approximation most of the time, since the signal is not perfectly periodic in N . Applying the DFT is like an assumption that the signal has and will continue as an exact replication of the measured interval. This copy and paste procedure creates an error referred to as leakage. The signal is cut off at both ends, leading in a periodically replicated error [3]. The DFT has two peaks, both being lower than the correct value.

Also, if the frequency increment ($1/t_{meas}$) is too low, the spectrum might not have a frequency line at the exact peak frequency [3]. So the energy will be distributed to neighboring peaks, leading to the same problem.

As the signal is time-limited, we can consider it to be cut off by its multiplication with a rectangular window function. Windowing functions are sometimes multiplied with the time domain signal (and have the same length) in order to diminish the effect of leakage. The error issuing the cutting off is diminished as the beginning and end of the signal are weighted less than the middle values. Windowing has the disadvantage of falsifying the peak magnitude, requiring a correction. Also two neighboring peaks might be impossible to be told apart. As the measurement time in the following experiments is mostly five to ten seconds, the resolution of 0.2 Hz / 0.1 Hz is sufficient. A window is not applied to the signal, as a hanning window was tested and found not helpful. The peaks are pretty clean for the following measurements, as the pressure field is mainly determined by the (chosen) input frequency.

4.2 MATLAB code for analysis

The following code demonstrates the procedure followed for each measurement. It includes the following steps:

- import data
- define sampling frequency of measurement
- define frequency of signal (known from frequency generator, required for 2 mic method)
- define parameter such as c , k , microphone positions
- define microphone sensitivities and convert (V) to (Pa)
- detrend signal by subtracting the moving mean
- FFT transform of the signal
- use the two microphone method to get the amplitudes A and B using two of the three microphones
- convert the x-axis from BINS to frequency
- plot the amplitude A over frequency
- use of the peak detection function to find the maximal value (showing at excitation frequency)
- save it in a matrix

All these steps have to be repeated for each measurement of phase and experimental setup.

For the next chapter all the maximal values corresponding to A and B are determined as described and plotted out of the matrix into a scatterplot. The spin ratio is calculated for each phase angle and plotted over the phase.

The following code serves as an example for one $\phi = 90^\circ$ measurement:

```

1 %code to get amplitudes A, B
2 %-----
3 A=importdata('90.txt'); %txt file containing the DAQ data
4 %-----
5 fs = 51200; % sampling frequency
6
7 t=A(:,1); %time samples in first column
8 Number = length(A);
9 Number/round(t(end)) %verify sampling frequency
10 %-----
11 f=763; %frequency of measured signal, needed to get A and B
12 c=343; %speed of sound
13 k=2*pi*f/c; %wave number
14 %-----measurement points-----
15 x2=0.178; %measuring spot mic 2 in (m)
16 x3=0; %measuring spot mic 3 in (m)
17 %-----Microphone sensitivities-----
18 sens2=0.00413;
19 sens3=0.00407;
20 sens5=0.00413;
21 MIC2=A(:,2)/sens2; %get values and convert to (Pa)
22 MIC3=A(:,3)/sens3;
23 MIC5=A(:,4)/sens5;
24 %-----
25 n=1000; %window size for moving mean correction
26 MIC2=MIC2-movingmean(MIC2,n);
27 MIC3=MIC3-movingmean(MIC3,n);
28 MIC5=MIC5-movingmean(MIC5,n);
29 %-----FFT-----
30 MIC2_FFT=fft(MIC2);
31 MIC3_FFT=fft(MIC3);
32 MIC5_FFT=fft(MIC5);
33 %-----two microphone method -----
34 [amplitudeA_FFT,amplitudeB_FFT]=calculate_back(MIC3_FFT,MIC2_FFT,x3,x2,k);
35 amplitudeA_FFT=abs(amplitudeA_FFT); %get amplitude abs
36 amplitudeB_FFT=abs(amplitudeB_FFT);

```

```

37 %-----
38 N=length(t);
39 bin_vals = [0 : N-1];
40 new = bin_vals*fs/N;           %convert BINS to frequency (x-axis)
41 N_2 = ceil(N/2);
42 %-----plot amplitudes FFT-----
43 figure
44 plot(new(1:N_2),amplitudeA_FFT(1:N_2))
45 xlabel('time')
46 ylabel('amplitude');
47 title('FFT Amplitude A ')
48 xlabel('Frequency [Hz]')
49 %-----peak detection to find value for excitation frequency-----
50 delta_A=100000; % value has to be so high as the magnitude is
51 delta_B=100000; % not scaled (2/N) yet
52
53 [MAXTAB_amplitudeA] = peakdet(amplitudeA_FFT, delta_A);
54 [MAXTAB_amplitudeB] = peakdet(amplitudeB_FFT, delta_B);
55 %-----
56 MATRIX=[MAXTAB_amplitudeA(1,:), MAXTAB_amplitudeB(1,)]/N*2;
57 %matrix containing the bin number and its value
58 % *2/N scales the pressure to (Pa) as explained above
59
60 % HERE various plots can follow to illustrate the results

```

As described in [2] the values of all three microphones could be used to determine A and B more accurately. The system would then be overdetermined, so that the least squares method would minimize the error. For the following results only two microphones are evaluated. The least squares method should lead to improved results and is recommended for further investigation.

Chapter 5

Results and discussion

Once the equipment is mounted, tested and familiarized with, a set of configurations is experimented with, in order to better understand the nature of acoustic oscillations in annular combustors. The frequency generator is connected to the amplifiers which are connected to the speakers in turn. The voltage that reaches the speakers is measured using the RMS-function of a multimeter and then adjusted with the frequency generator to eliminate the amplifiers as source of errors. For all the setups the amplitudes A and B have been calculated using the two microphone method described in the previous chapter (4).

5.1 Assumptions

Some assumptions had to be made for this work. They are necessary to apply the presented method:

- The modes are not changing with air flowing in the case of acoustic driver excitation, as the source (speaker) as well as the receiver (microphone) are not moving relatively to one another [11]. While characterizing the modes using speakers, the air flow will not affect the results. This will, however, be the case for thermoacoustic instabilities, as the heat source fluctuates and the flames move.
- The waves travelling around the duct (described in section 2.1) are assumed plane waves. For the more complex situation of the annular chamber, there is no obstacle stopping the pressure waves from expanding into the room above it. While the non-ideal pressure waves expand in the chamber, they are reflected and propagate outside

the chamber. These propagation losses might be decisive for the shapes observed in the following figures (e.g. 5.10). A complete description of the sound field would require numerical simulations. Within the frame of this work, it is assumed that the sound field can be approximated as two plane waves travelling around the annulus. Due to this simplification, the results of the measurements have to be interpreted with even greater care.

- The two microphone method is assumed to be sufficient to describe the sound field in a combustor as well as it does in a Kundt's tube. For this evaluation only microphones 3 and 2 have been evaluated. Microphone 3 is located (if not specified in the section) right under one of the speakers, while microphone 2 is placed 120° from it in anti-clockwise direction. The evaluation would be more precise if the least squares method, evaluating all three microphones and minimizing the error (described in [2]) would have been implemented.

5.2 Goal: standing, spinning and mixed modes

Regarding the analogy between the Kundt's tube and the annular chamber, it can be concluded that an excitation with the first eigenfrequency with one speaker should result in a standing wave. By exciting with the same amplitude and varying the frequency in a continuous linear sweep, the eigenfrequency can be identified. It is within the range of what could be expected due to geometry.

The inner and outer circumference of the combustor are calculated below. So is the mean diameter, which the microphones are located on.

$$C_i = \pi D_i = \pi \cdot 13cm = 40.8cm$$

$$C_o = \pi D_o = \pi \cdot 21cm = 66cm$$

$$C_m = \pi D_m = 53.4cm$$

One third of C_m is the distance between the microphones used in the evaluation, as the microphones are placed at the mean diameter under the chamber in the tubes 2.10.

$$\lambda_{eigen} = \frac{c_{mean}n}{f_{eigen}} = 44.95cm \text{ for } n=1$$

$$C_i < \lambda_{eigen} < C_o$$

$$f_o < f_{eigen} < f_i$$

The resonant frequency corresponds to a wavelength which can be pictured as a circumference of the curved travelling wave. The equations above show that the wavelength is in-between the inner and outer circumference. It should be noticed that it is closer to the inner circumference. That might be the result of the waves being bended, but could not be fully understood.

If a second speaker gets the same frequency and at the same phase, the superposition of the two waves will result in new amplitudes A and B. Changing the speakers' relative signal phase in steps will change A and B and move the point (A;B) in the scatter plot 5.1. A mixed mode should occur due to summation and/or cancellation of the four waves (two in opposite directions for each speaker). The clockwise rotating waves originating two different speakers will e.g. sum up, while the anti-clockwise rotating waves will cancel, depending on the phase angle. These four waves can be described as two waves resulting the superposition.

The aim of this work is to excite the combustor in a way that demonstrates standing, spinning and mixed waves. To characterize the nature of the mode, the spin ratio (SR) is used.

$$SR = \frac{|A| - |B|}{|A| + |B|}$$

If A is twice as high as B or the other way around, the SR becomes $\pm\frac{1}{3}$. Just as in [19, 20] the mode is described as:

- predominantly standing: $-\frac{1}{3} < SR < \frac{1}{3}$
- spinning clock wise: $SR > \frac{1}{3}$
- spinning anti-clock wise: $SR < -\frac{1}{3}$

These definitions correspond to areas in the amplitude scatterplots (fig. 5.1) and spin ratio plots (fig. 5.2).

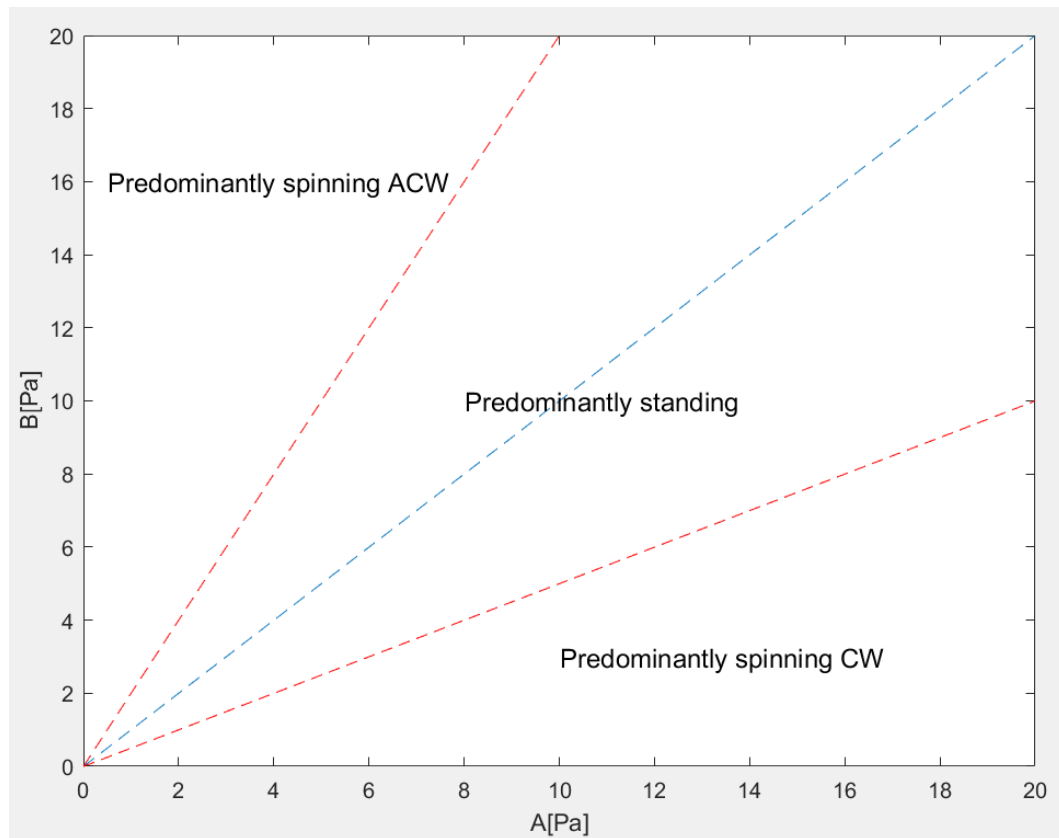


Figure 5.1: Mode characterisation: scatterplot amplitudes A and B

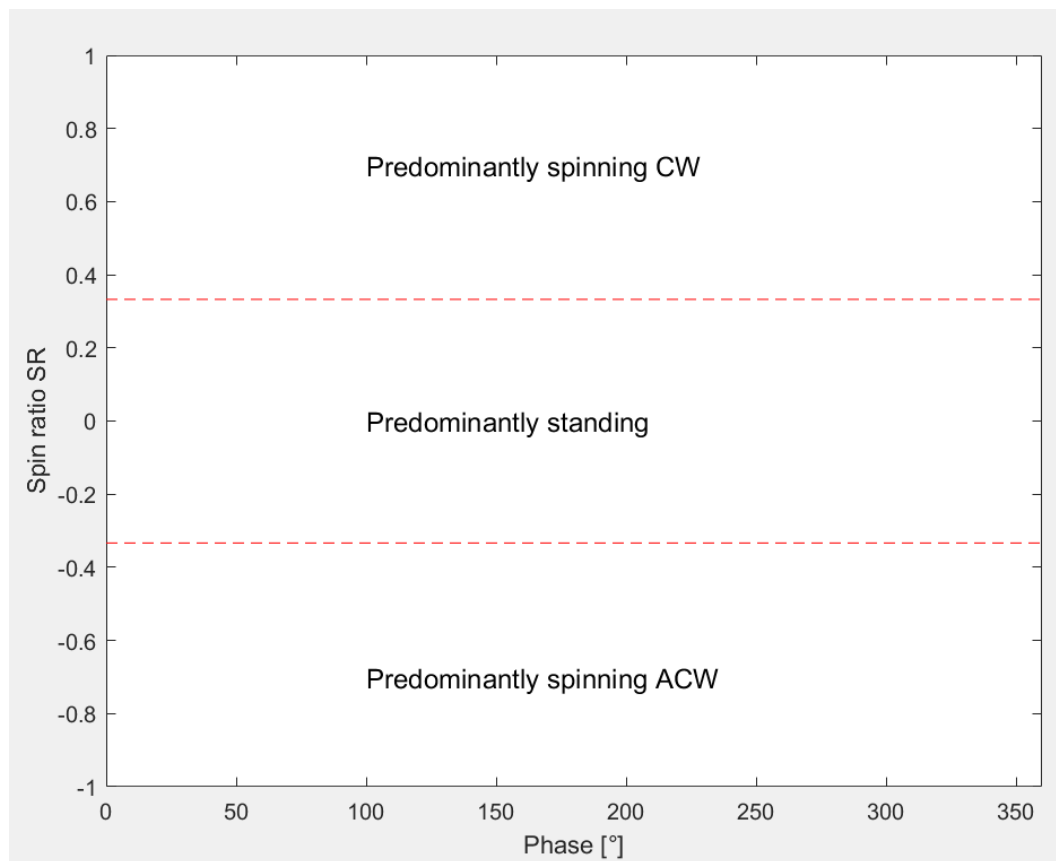


Figure 5.2: Mode characterisation: spin ratio

5.3 Microphone influence

The calibration of the microphones has partially been discussed in section 2.4. The testing setup is as shown in figure 5.3. The microphones have been exposed to the same sound field in the combustor chamber (one after another) at the same position. The RMS voltage of the speaker input was checked with a multimeter. Each measurement lasted five seconds. While one microphone was tested, the other microphones were positioned in the other two tubes.

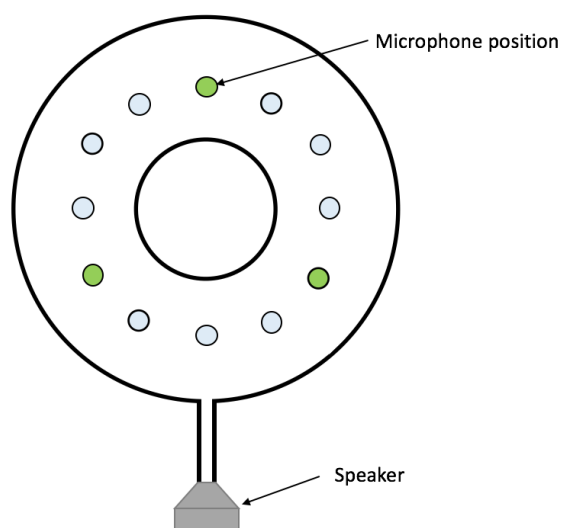


Figure 5.3: Setup for microphone calibration measurements

The pressure signals have been FFT transformed and the peak values (at excitation frequency) have been compared. The use of the peak value of the FFT eliminates surrounding noise, as only the frequency of interest is considered. If the RMS of the time signal was used instead, unwanted noise would be included. Assuming the mean peak value of the three microphones as correct (the correct value is unknown), the error for each microphone in percent relative to the mean has been calculated. For the frequency of interest it is under 1 percent, but for high frequencies, usually including higher damping, the error is up to 8 percent (table 5.1). This might be due to differences in the sealing with a rubber ring, which is important according to [4]. It appears that some rubber rings are more worn out than others, which could explain the high discrepancies at higher frequencies.

Calibration microphones				Error rel. to mean amp			
Exc. frequency	Mic2 amp	Mic3 amp	Mic5 amp	Mean amp	Mic2 %	Mic3 %	Mic5 %
250	0.30559	0.30916	0.30428	0.30634333	-0.2459115	0.91944768	-0.6735362
500	0.31002	0.32014	0.30975	0.31330333	-1.0479727	2.18212382	-1.1341511
750	8.741	8.8132	8.7247	8.75963333	-0.2127182	0.61151722	-0.398799
760	10.126	10.253	10.107	10.162	-0.354261	0.89549301	-0.541232
1000	0.91695	0.94889	0.94951	0.93845	-2.2910118	1.11247269	1.17853908
1250	0.85143	0.87844	0.89155	0.87380667	-2.5608258	0.53024697	2.03057885
1500	3.2403	3.4479	3.2476	3.31193333	-2.1628857	4.10535639	-1.9424707
1750	1.4655	1.644	1.6771	1.59553333	-8.149835	3.03764676	5.11218819

Table 5.1: Microphone calibration results

To make sure the microphone calibration is sufficient for this investigation, measurement C from section 5.10 is evaluated. Two speakers are 90° apart from each another. Their signals (sine 763 Hz) are phase shifted in steps. First, the pressure is evaluated as measured. Then there is a test error included. The signal of microphone 2 is multiplied by 0.99, whereas the signal of microphone 3 is multiplied by 1.01. Again, the measurement is evaluated. This approach assumes the most unfavorable case of a high Δp , as one mic measures “too much” and the other “too little”. As can be seen in figures 5.4 and 5.5, the shape and spin ratio are nearly unaffected by the errors.

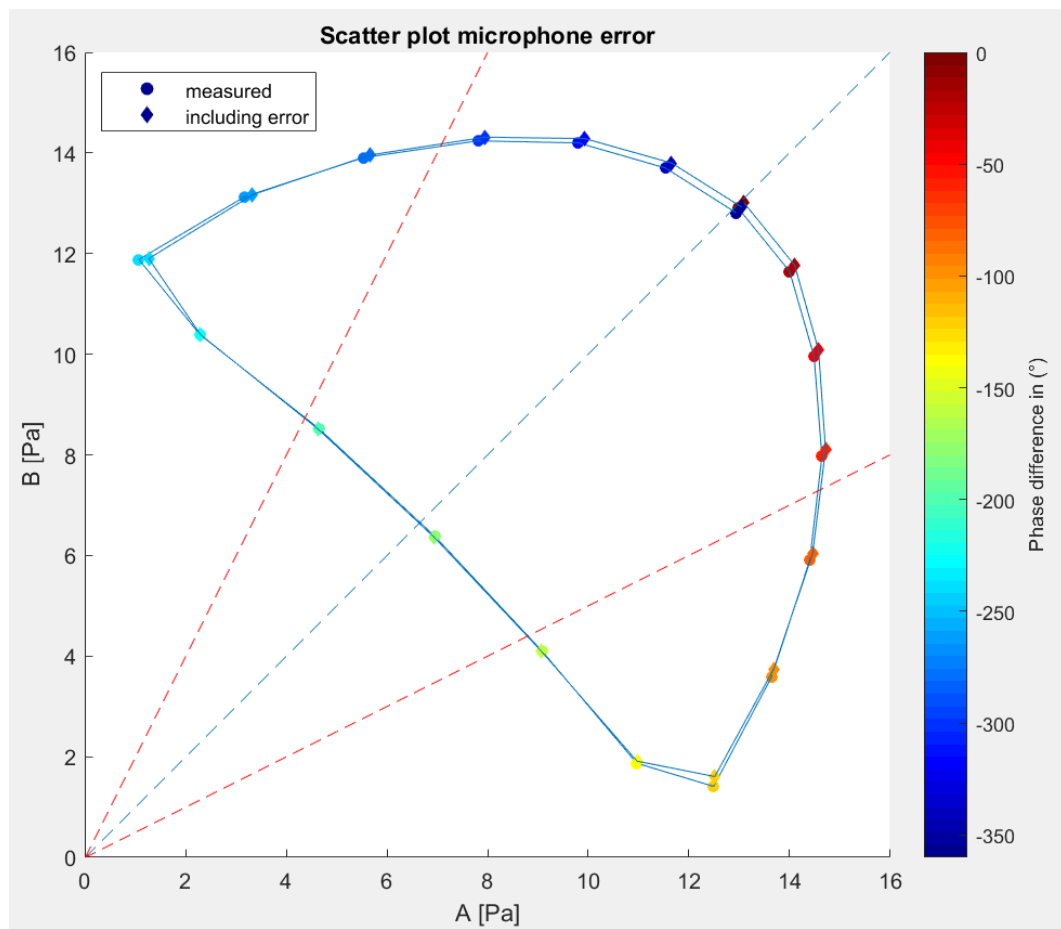


Figure 5.4: Scatterplot comparison: normal and with microphone calibration error

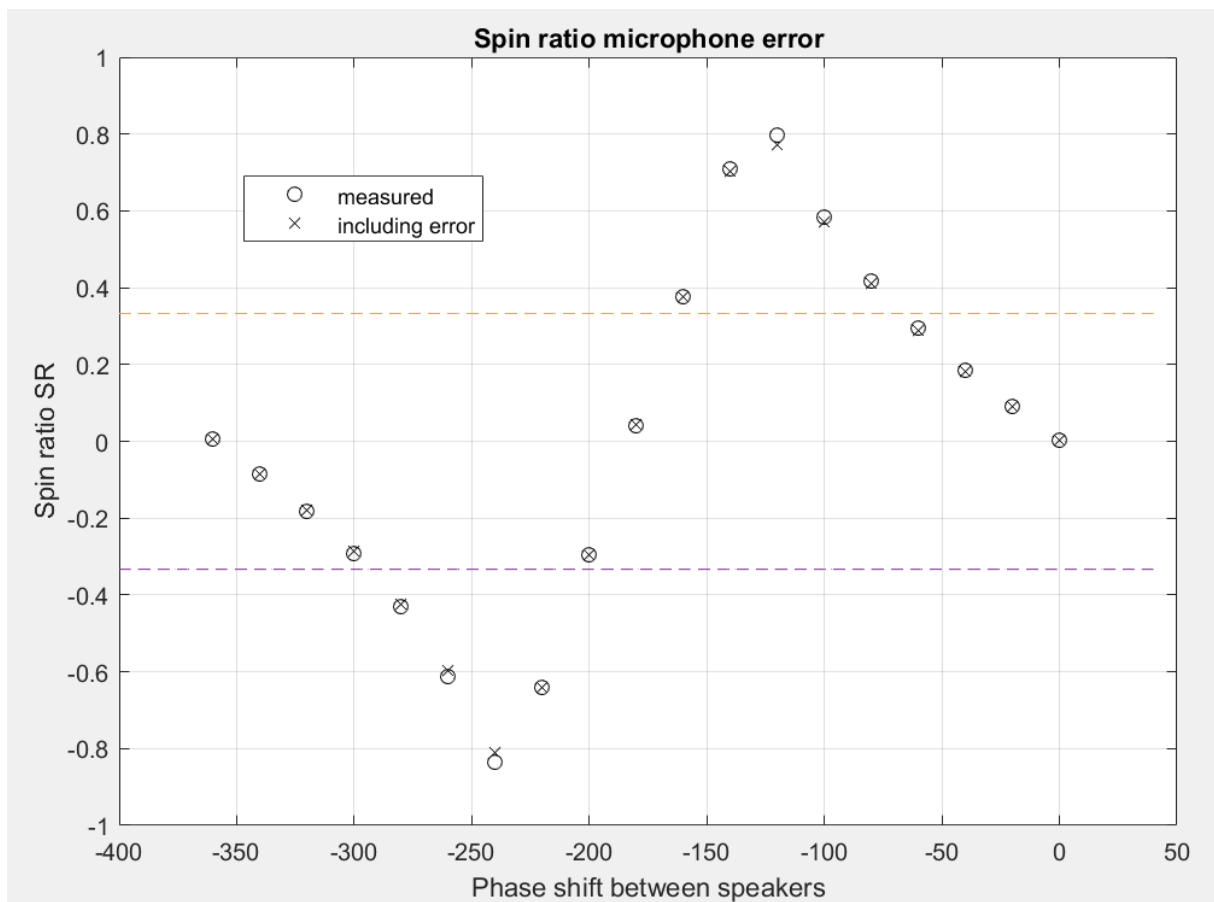


Figure 5.5: Spin ratio comparison: normal and with microphone calibration error

This work's purpose is to investigate the possibilities of controlling the modes. Even with the microphone error, moderate control is possible. A finer tuning of speakers and microphone will however be necessary if the control aims to be more precise.

5.4 Speaker influence

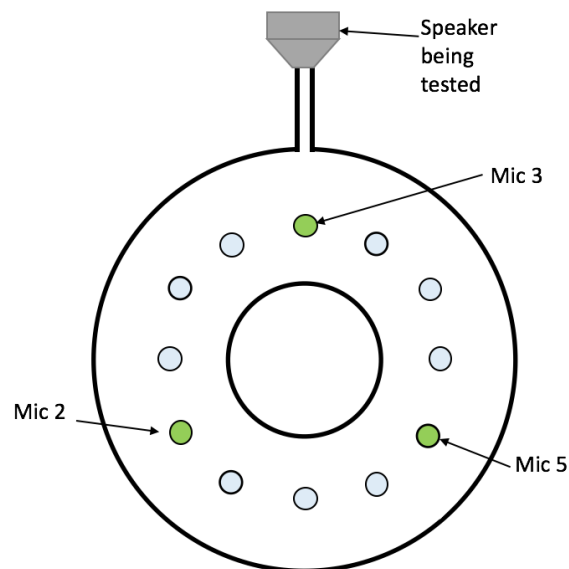


Figure 5.6: Setup for speaker calibration measurements

To test whether the identical acoustic drivers (speakers) are actually behaving the same way if exposed to the same input, the pressure field in the combustor has been measured for two different speakers placed at the same location with the same input. A multimeter was used to check the RMS input voltage. The input signal was a sine of 763 Hz, the first eigenfrequency. Previous measurements showed that the speakers might have an influence, even though they are supposed to be identical. As the evaluation of data shows (table 5.2), the amplitudes measured for the two speakers, using all three microphones, are quite different.

Calibration speakers	Mic 2	Mic3	Mic5
Speaker 1	4.5098	10.852	6.0243
Speaker 3	4.3659	11.334	6.4848
Mean	4.43785	11.093	6.25455
Error of speaker 1 in % rel. to mean	1.62128058	-2.1725412	-3.68132
Error of speaker 3 in % rel. to mean	-1.6212806	2.17254124	3.68132

Table 5.2: Speaker calibration: error relative to mean pressure for each microphone

The pressure signals were FFT transformed and the peak values of the microphones for 763Hz were compared. When admitting the mean value between speaker 1 and speaker 3 as correct and dividing the difference in magnitude between each speaker and mean value by the mean value, the error is around 1.6 percent for microphone 2 and around -2.2 percent for microphone 3 and around -3.7 percent for microphone 5. A valid conclusion is that the speakers would require further investigation to get more accurate results. The fact that the amplitude is higher for one microphone and lower for the two others, makes it improbable to establish a meaningful correction for the speakers. The setup indicates the highest values for microphone 3 (located under the speaker) and lower values for microphone 2 and 5. As can be seen in table 5.2, the values of microphone 5 are considerably higher than for microphone 2, which could indicate a geometrical inaccuracy, leading the waves more into one direction around the annulus than into the other. Similar indices for such a behaviour will be discussed in section 5.9 and 5.10.

Figure 5.12 (in section 5.7) illustrates how the results are modified by one speaker emitting higher pressure waves than the other. If we look at the positions of a ten percent difference, we can conclude (like for microphone calibration) that the shape of the curves will be affected.

All the results from now on should, however, be considered with regard to speaker and microphone calibration. There is a falsification of the results issuing this, but the results still show some interesting and reproducible effects.

5.5 Eigenfrequency determination

The frequency generator is used to do an automatized linear sweep from 200 to 2000 Hz lasting 100 seconds. Microphone 3 is used for evaluation as it is located above the speaker. As there is an anti-node at that position the amplitudes are highest. The combustor is excited with white noise in another measurement (not displayed here). The excitation with white noise aims at stochastic resonance and was used to counter-check the shape of the curve.

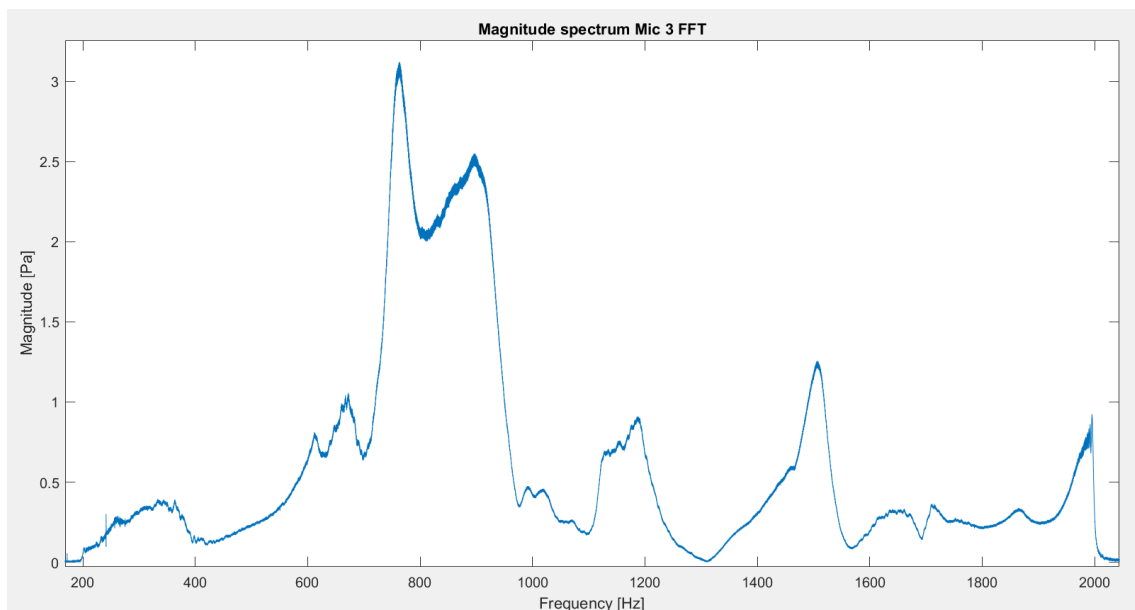


Figure 5.7: Frequency sweep, 100s, 200-2000Hz: FFT of pressure response

The sweep curve indicates a peak between 760 and 765 Hz. As the eigenfrequency could not be determined clearly, it has been varied between 760 and 765 Hz. As a matter of fact, the attempts to measure the response in 1 Hz steps between 760 and 765 Hz showed different results depending on the microphone evaluated. The best approximation is assumed to be 763 Hz, which was used for most of the following measurements. It is the peak frequency for microphone 3, which is located right under the speaker, as mentioned above.

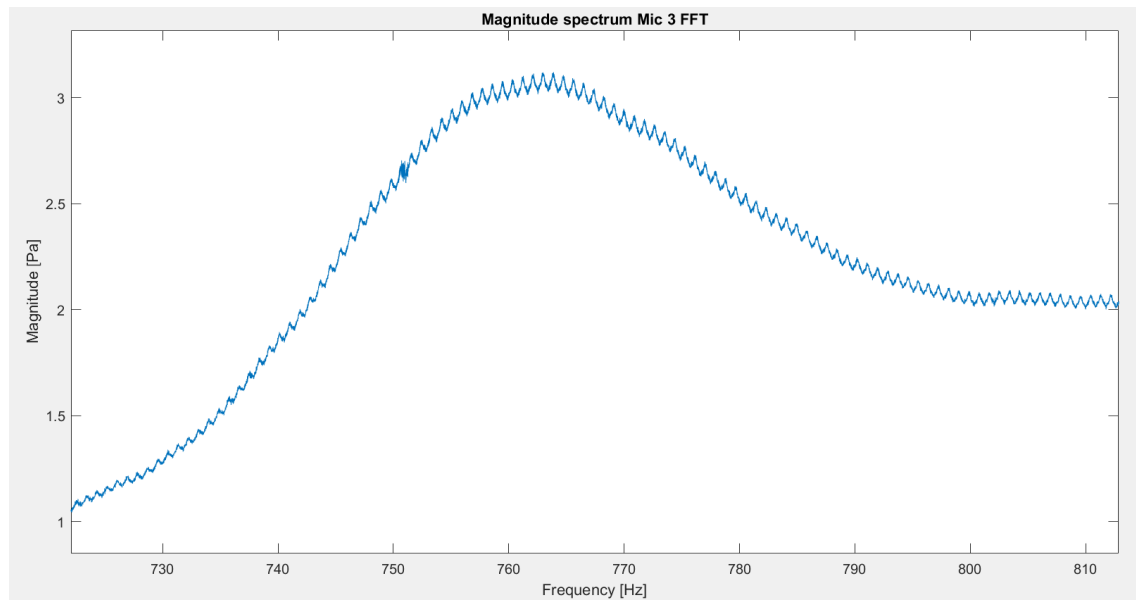


Figure 5.8: Frequency sweep in detail

The peak frequency is identified as corresponding to a circumferential standing mode, as $A \approx B$ (displayed in the following sections).

5.6 Influence of the forcing amplitude

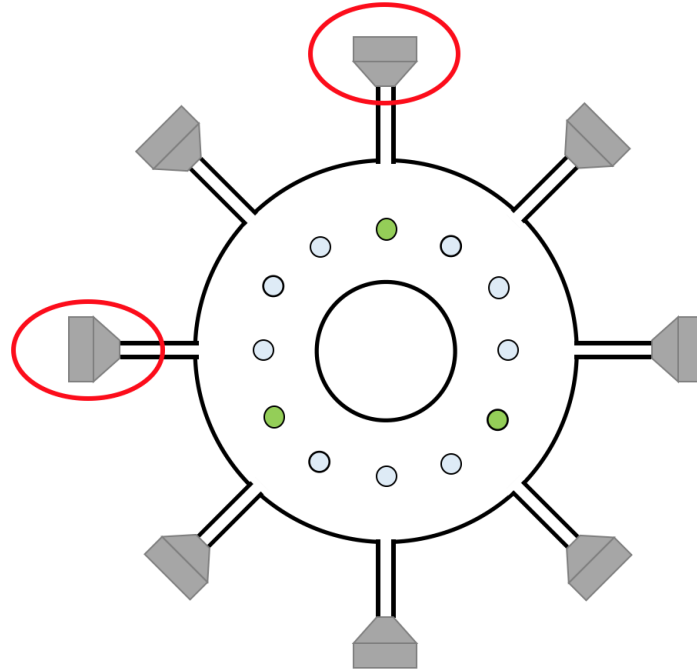


Figure 5.9: Setup 90° between used speakers

Figures 5.10 and 5.11 show how varying the phase between two speakers with 90° spacial angle (fig. 5.9) will affect A and B as well as the spin ratio. The initial amplitude in the frequency generator (run at 760 Hz) was chosen to be $1 V_{pp}$ (peak to peak meaning 0.5V amplitude). It was then increased to $2V_{pp}$ and $3V_{pp}$ (for both speakers). The maximum of $3V_{pp}$ is chosen to limit the noise the author was exposed to during the experiment series. For each of these amplitudes, the phase was varied in -10° steps to see how this would affect the sound field. Each measurement lasted ten seconds. As can be seen, the amplitudes A and B vary with the phase. For the first ten steps, the spin ratio increases and reaches a maximum at around -120° .

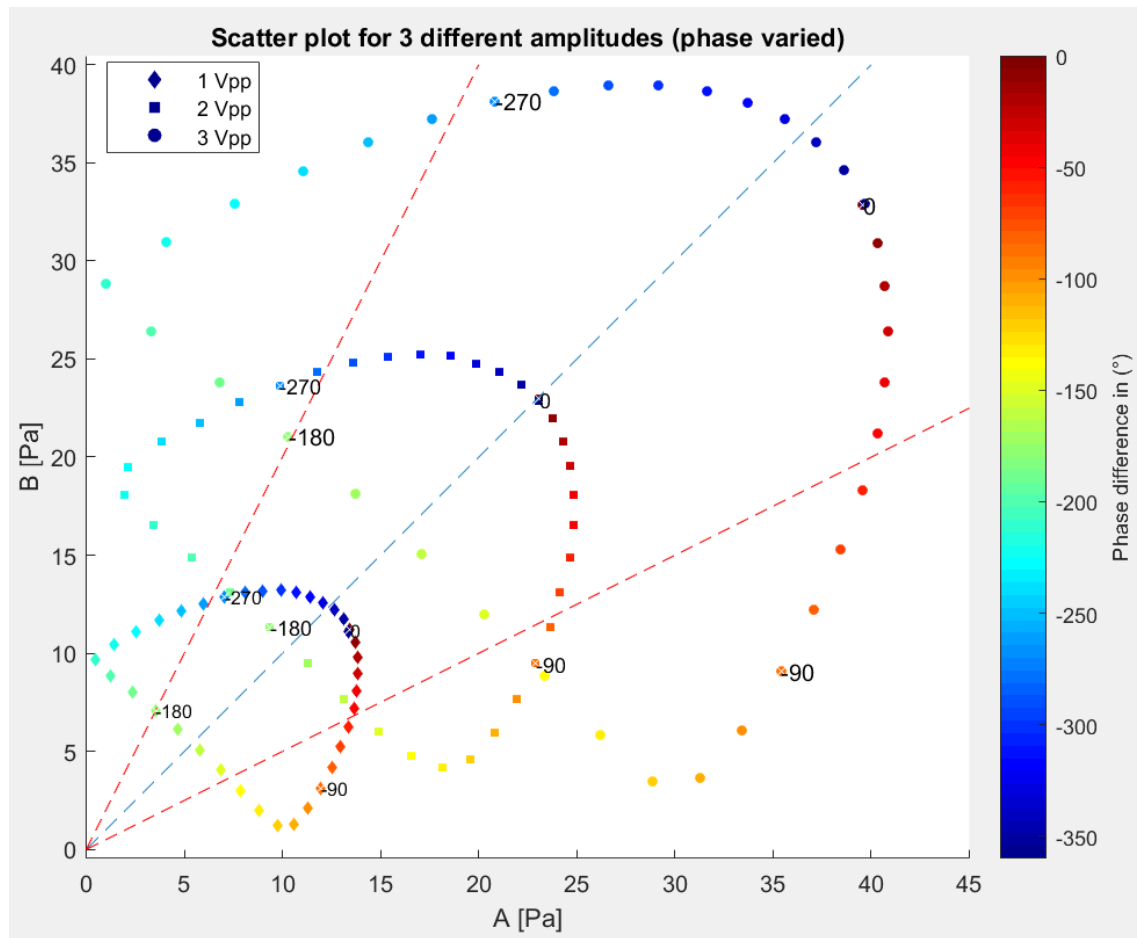


Figure 5.10: Scatterplot for three different amplitudes (pointsize) and 10° phase steps

Several things are remarkable:

- There is a gap between 0° and 180° . The waves partially cancel or sum up, depending on the spin direction.
- $0^\circ/180^\circ/360^\circ$ are not perfect standing waves but slightly off the $A=B$ line. B is smaller than A even though they should be identical due to symmetry. That might indicate geometric inaccuracies.
- The shape of the curve does not vary a lot with forcing amplitude. It is mainly a repositioning of the half-moon shaped curve towards higher or lower amplitudes.

The similarity of the three curves shows that an increase in amplitude leads to quite pre-

dictable results. It is possible to control A and B within the limits of the the maximal (around 0.8) and minimal (nearly -1) spin ratio. The influence of amplitude variation on the spin ration (fig. 5.11) itself seems negligible and is not expected from a theoretical point of view.

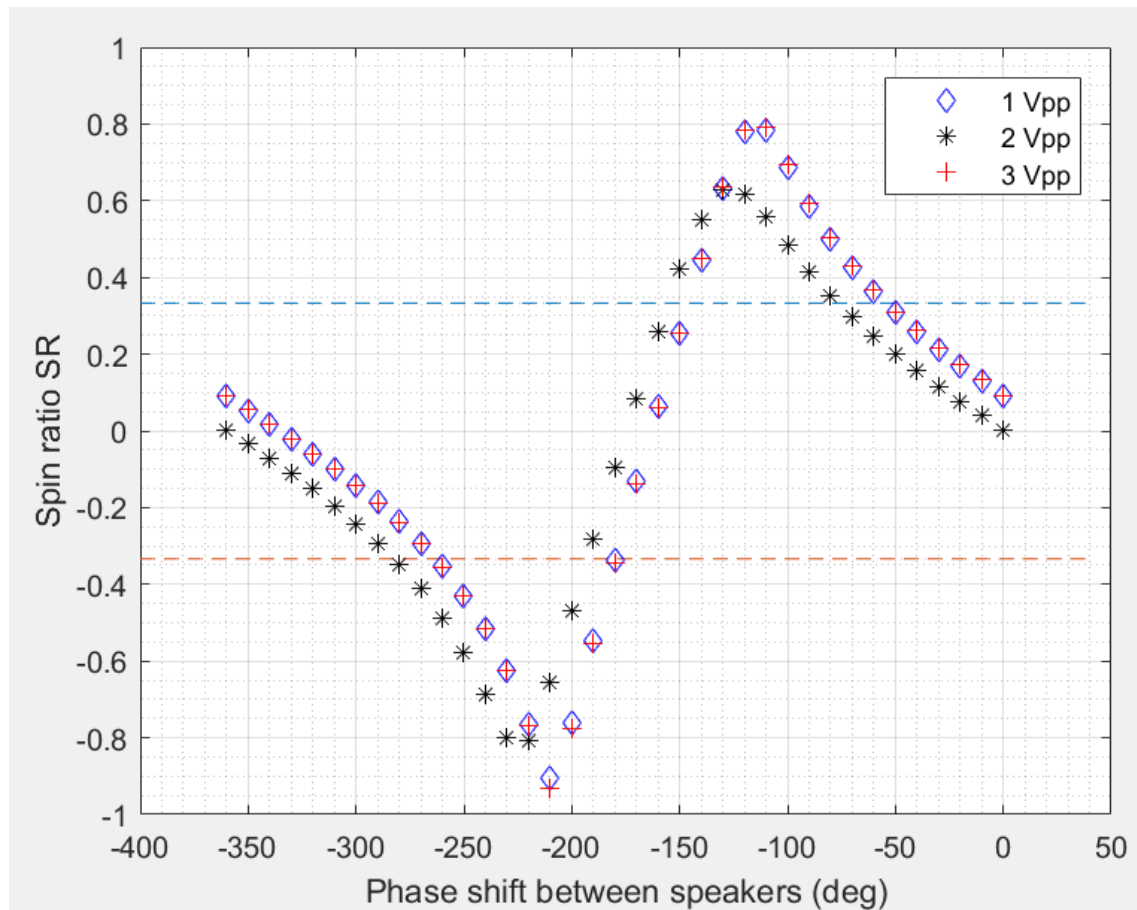


Figure 5.11: Spin ratio for three different amplitudes and 10° phase steps

5.7 Amplitude variation between speakers

In the previous setup, the amplitude of both speakers is varied at the same time. The following setup (763 Hz, 5 seconds measurements and 90° speaker angle) has the objective is to find out what happens if only one of the amplitudes is to be varied. The phase shift between the signals is 0° . Starting from a slightly lower amplitude at one speaker, the amplitude of that speaker is increased in steps. The increasing point size indicates increasing

amplitude. It can be seen that by the time the amplitude of one speaker is 3.6 times higher, the wave becomes almost perfectly standing, with A being equal to B. The speaker with lower input has almost no impact and is “drowned”. That also means that the speaker with higher almost nearly generates a perfect standing wave.

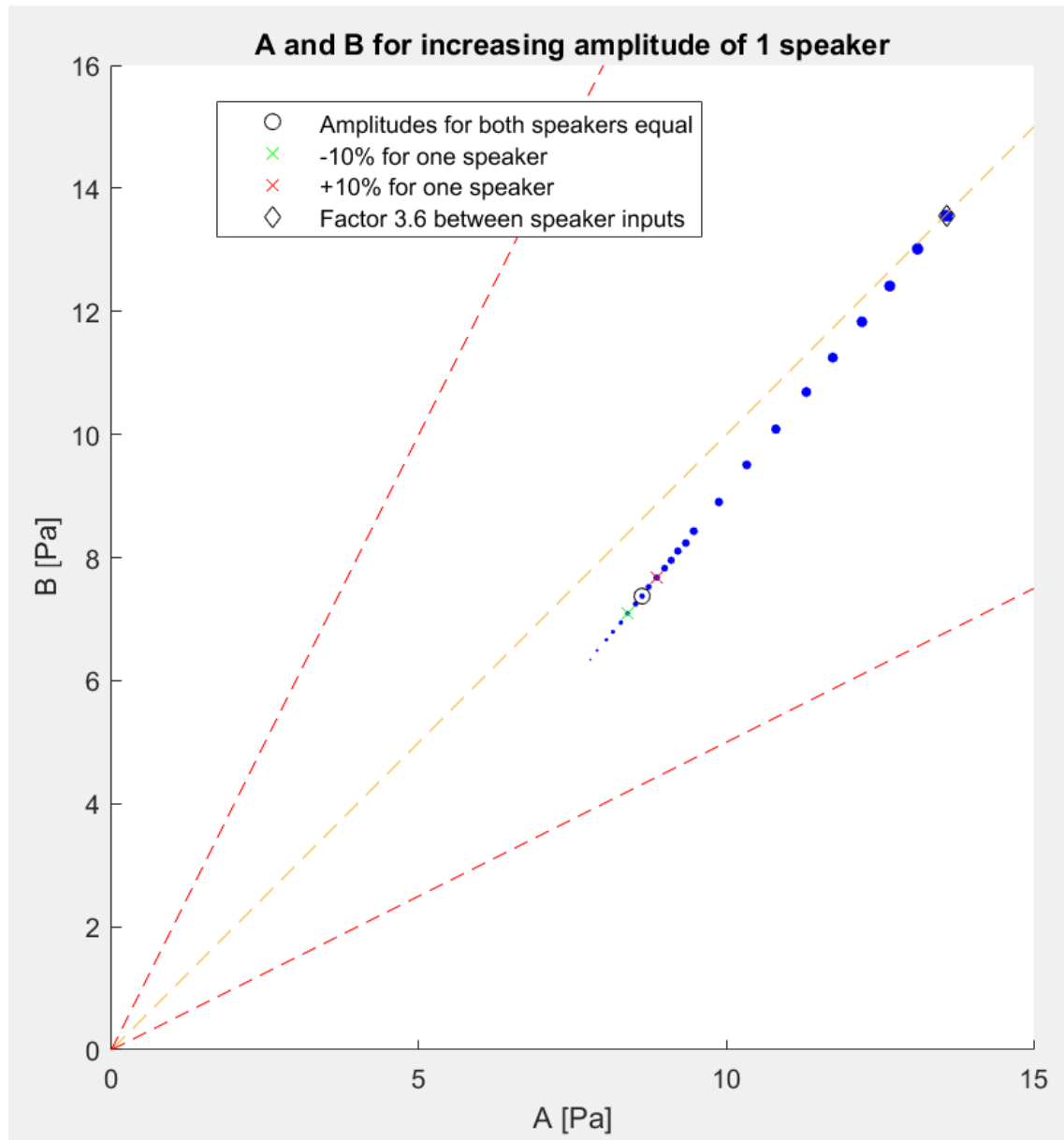


Figure 5.12: Increasing the amplitude of one speaker: error due to speaker differences

It seems that varying the amplitude of only one speaker is not helpful if spinning modes are to be created. To excite standing modes or to correct speaker influence it might be useful.

5.8 Influence of speaker position and phase angle

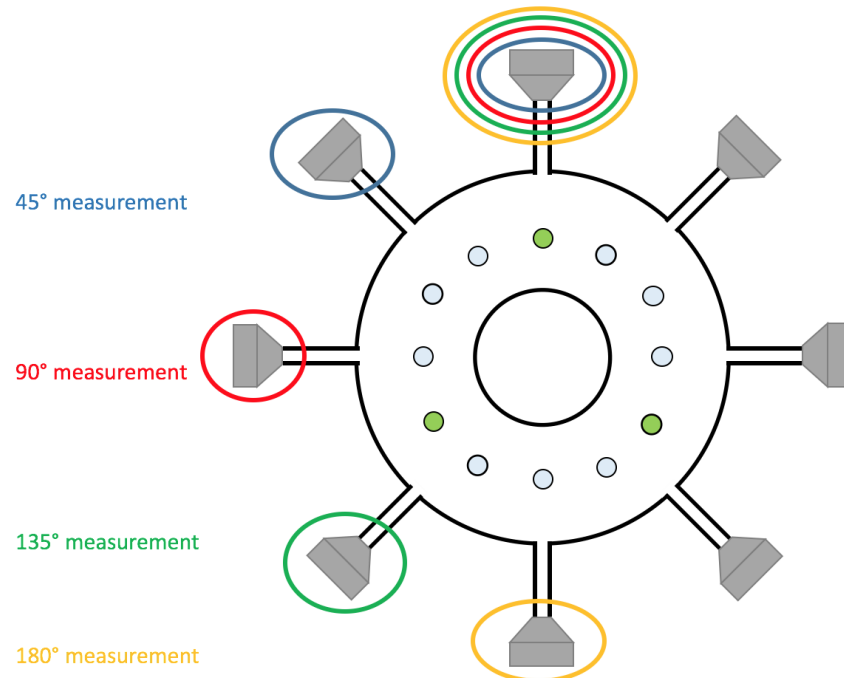


Figure 5.13: Speaker positioning for current setup

For these measurements one signal is sent to a fixed speaker. The second signal is sent to the speakers in positions 45° , 90° , 135° and 180° spacial angle, one after another, as displayed in figure 5.14. The speaker is a different one for each series of measurements. In the same way as in section 5.6, the phase between the signals was varied in steps of 10° for each position. The 763 Hz sine voltage signal was checked with a multimeter's RMS function to be identical. Each measurement of phase and position lasts ten seconds.

The purpose of this setup is to understand the influence of phase and relative speaker position onto the amplitudes A and B as well as onto the spin ratio.

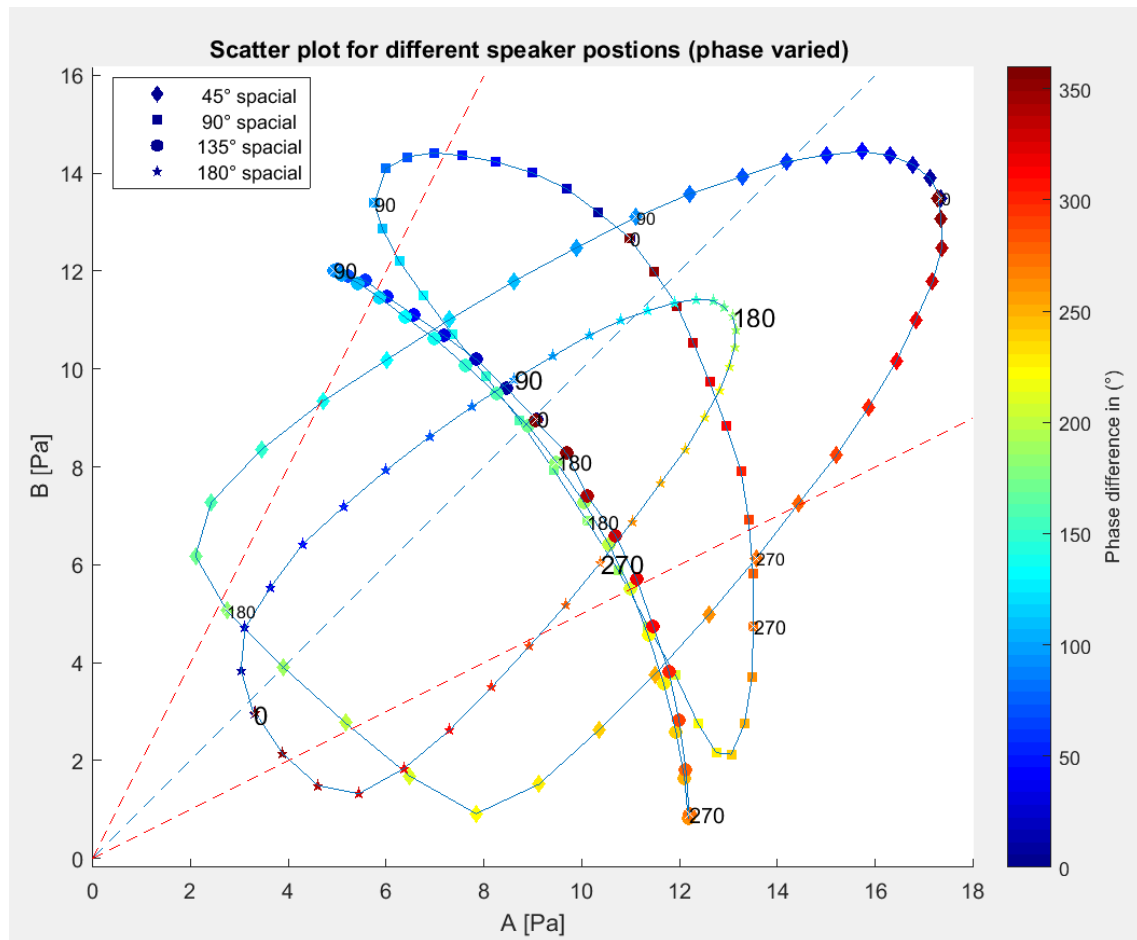


Figure 5.14: Scatterplot for different speaker positions and phases between signals

As can be seen in figure 5.14 there is a trend towards asymmetry just as already observed in section 5.6. Amplitude A tends to be bigger than B. The spinning ratio's values are thereby not covering the same interval in positive as in negative values (fig. 5.15).

The speaker position of 135° in figure 5.14 shows the most clean results. The amplitudes are quite predictable as the curve seems to be close to quarter a circle. If the amplitudes of both speakers are to be increased or decreased, most of the surface in figure 5.14 could be covered. Ideally, this would mean that any combination of A and B could be achieved, implying a perfect control of the sound field.

The shape of the curves indicates that, depending on the phase difference, there is partial cancelation or summation of the waves travelling around the combustion chamber.

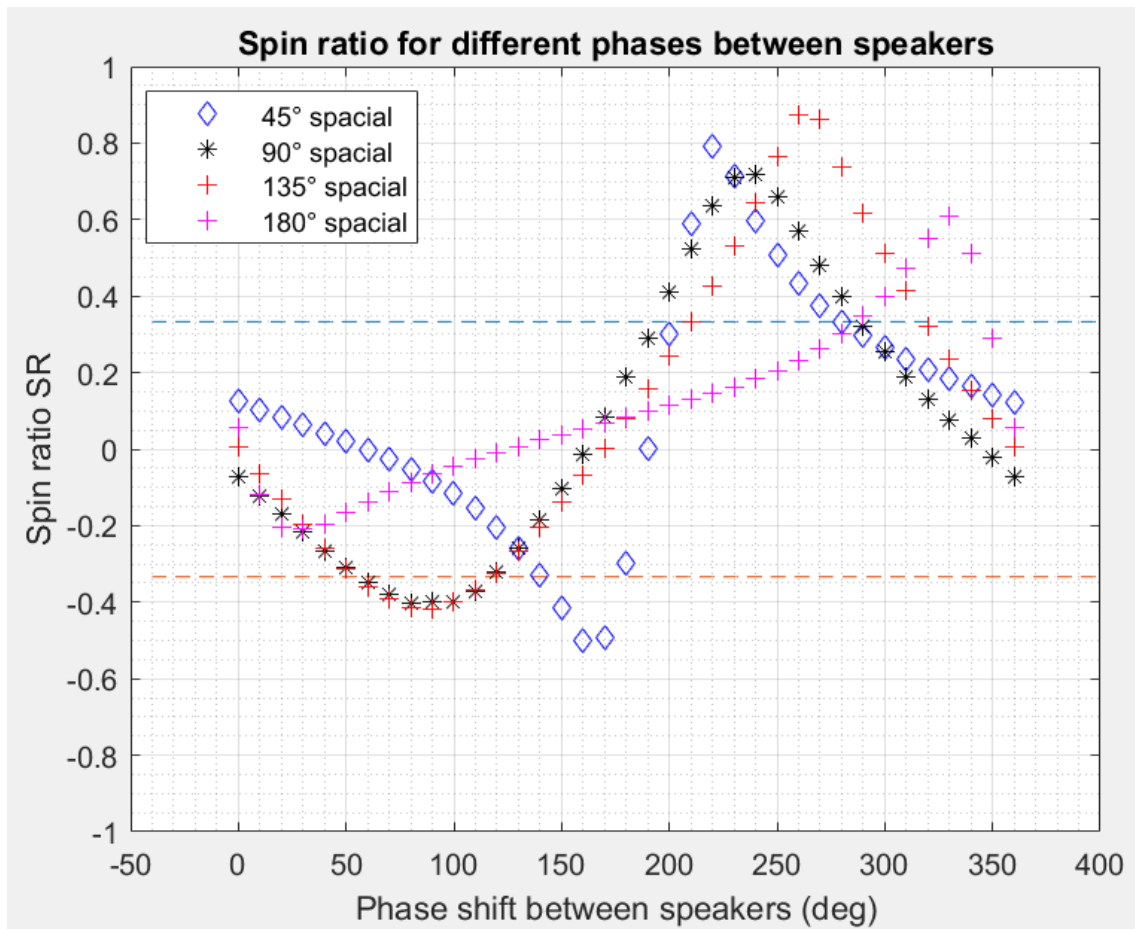


Figure 5.15: Spin ration for different speaker positions and phases between signals

All eight speakers were mounted during all experiments and in this case the cable was moved to 45° , 90° , 135° and 180° .

5.9 Influence of speaker position and phase angle 2

The setup is the same as in the previous experiment except for one thing. In this setup it is not the cable that was moved, but the actual speaker. By using the two same speakers in all the measurements the effect of the individual speakers is eliminated. That way more information on the effects of the speakers positions can be gathered. The measurements in 20° steps at 763 Hz each last 5 seconds.

The fact that the scatterplot curves are not symmetric might be a result of the rig's manufacturing tolerances. The gap between 0° and 180° is a result of the superposition of the phase shifted waves and might be influenced by the travelling distances of the waves. As the acoustic loss is expected to be dependent on the path in the annulus, the loss will probably affect the result. In the case of opposite speakers (180° angle) e.g., complete cancellation would be expected for a phase of 0° , but is not observed (fig. 5.16) [20].

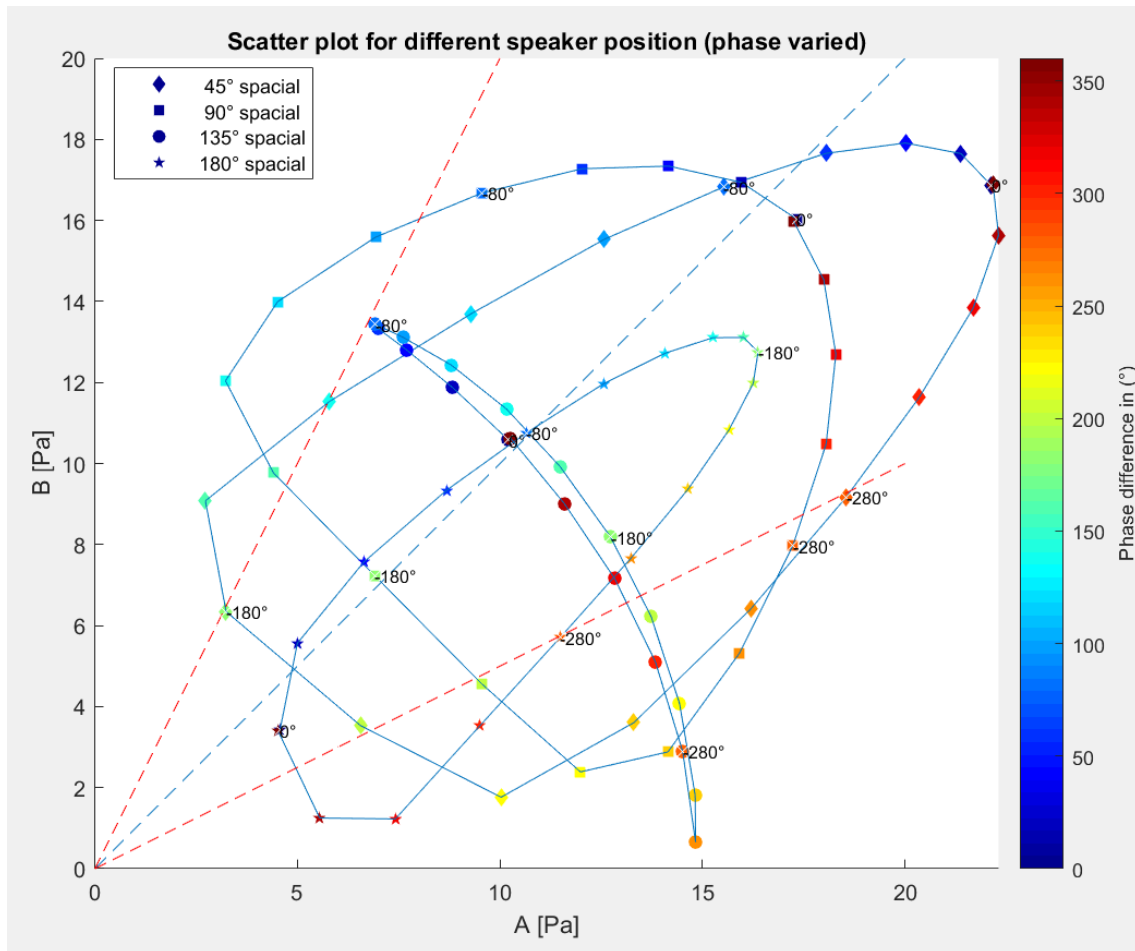


Figure 5.16: Scatterplot for different speaker positions and phases between signals (same speakers)

As in the previous setup the 135° curve seems to be the most interesting possibility to control the spin ratio in the combustor as it is most predictable. The difference in travelling distance between the two paths connecting the speakers ($3/8$ and $5/8$ of circumference) is lower than for 45° and 90° , but the setup is still asymmetric. Asymmetry might be required

to excite various mixed and predominantly spinning modes, as the 180° curve in figure 5.16 suggests.

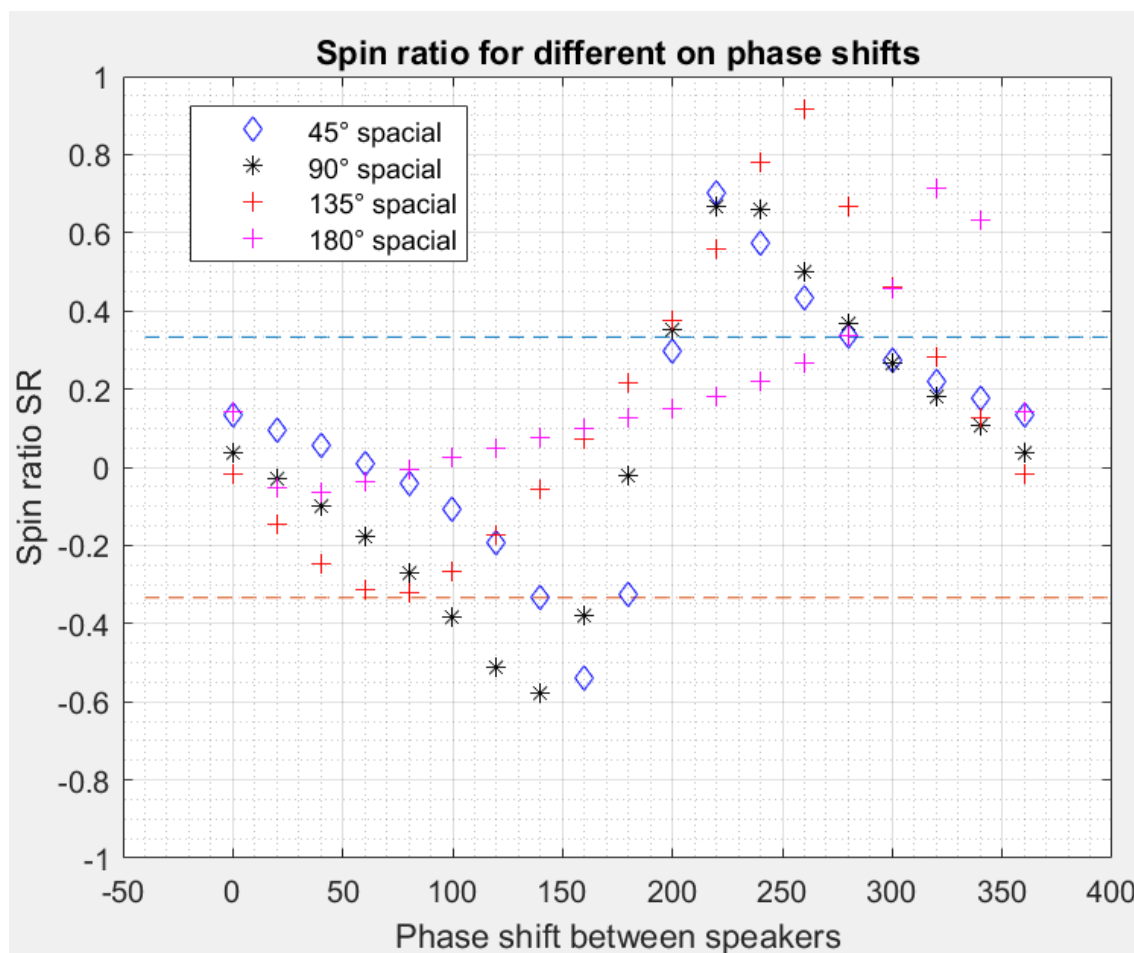


Figure 5.17: Spin ratio for different speaker positions and phases between signals (same speakers)

5.10 Influence of geometry

The last setup presented in this work aims to understand geometrical differences. The two same speakers are placed at different locations around the combustion chamber and fed with the same signal as for the previous measurement. Again the phase was varied for each of the four different position combinations A, B, C and D presented in figure 5.18.

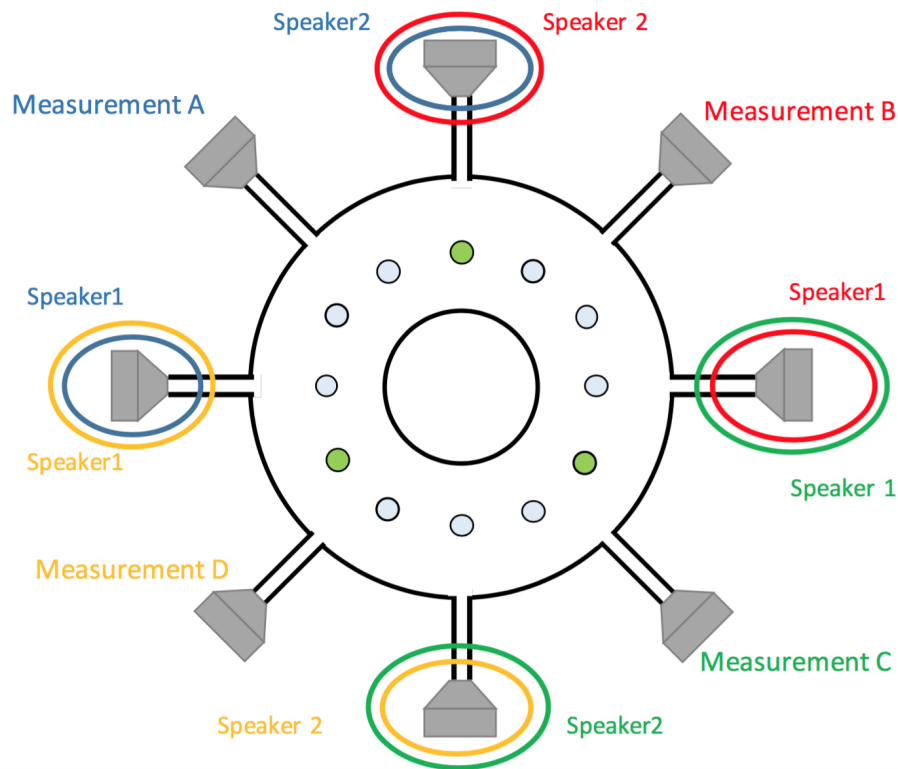


Figure 5.18: Different 90° speaker positions

For constellation A and C speaker 2 (no phase variation) was “leading”, while for constellation B and D speaker 1 (phase being varied) was “leading”. This difference in relative positions of the speakers one to another leads to a rotation of all the points around the half-moon center (fig. 5.19). The result is that the maximum amplitudes for measurement B and D do not occur at 0° phase shift but 180°. The reason for this could be the cancellation or summation of amplitudes travelling different paths. The role played by the acoustic loss in the shapes is unclear, but as the curves 135° earlier indicated, the gap between 0° and 180° phase angle grows with path (45°gap>90°gap>135°gap). Only as long as there is asymmetry (180° speaker angle means symmetry) this effect is observed (5.19).

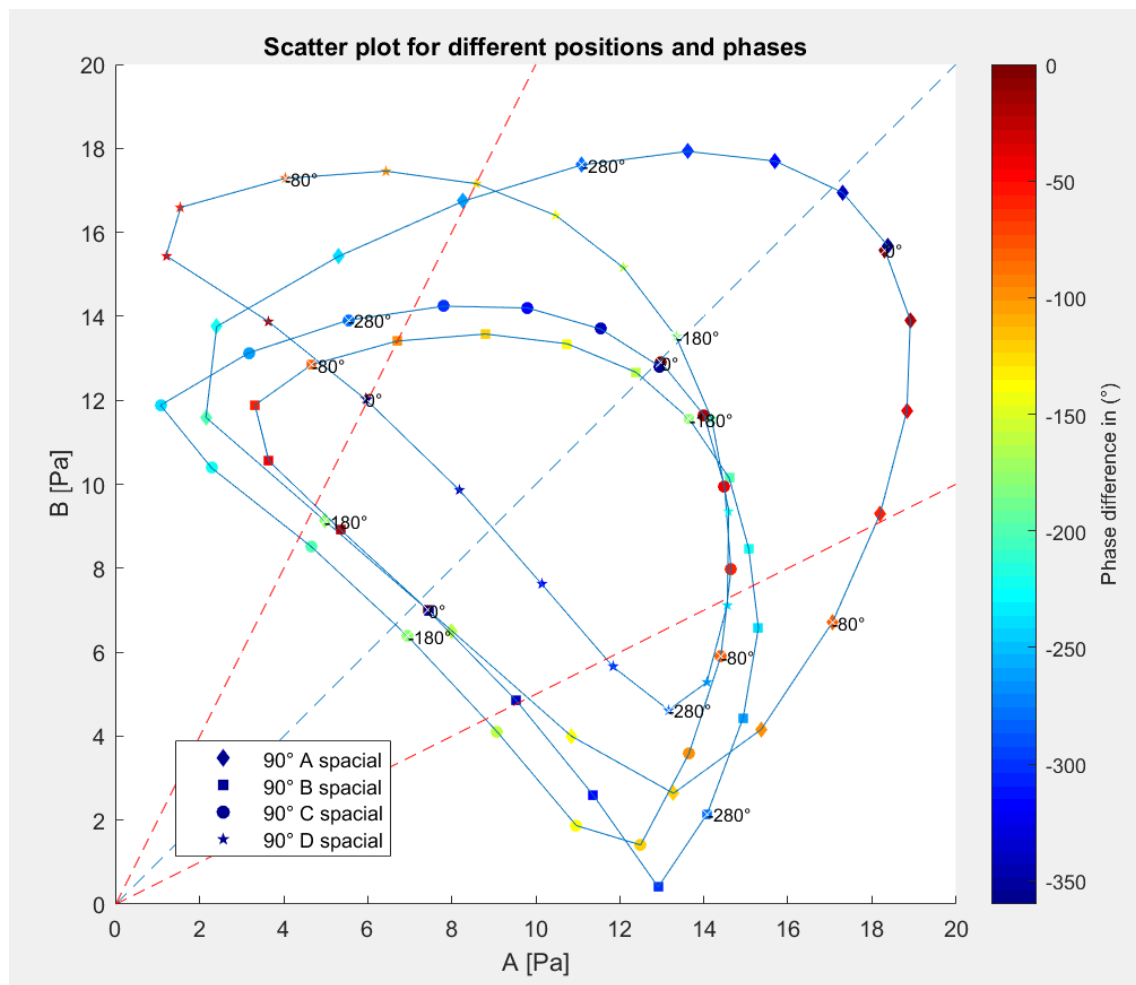


Figure 5.19: Scatterplot for different 90° positions and phases (same speakers)

Most importantly, the four curves are expected to look identical. As the input and the speakers are the same, the shape can only be caused by either the microphone positions or the rig's geometry. The microphones were not repositioned in this setup. Even though the two microphone method should help reconstruct the sound field no matter the speaker and microphone positions, an influence cannot be excluded.

The differences in shape and position between the curves could indicate that the tolerances of the rig might not be precise enough.

Finally, the spin ratio plotted over the phase shift once more illustrates the importance of the leading speaker and the differences between the four measurements:

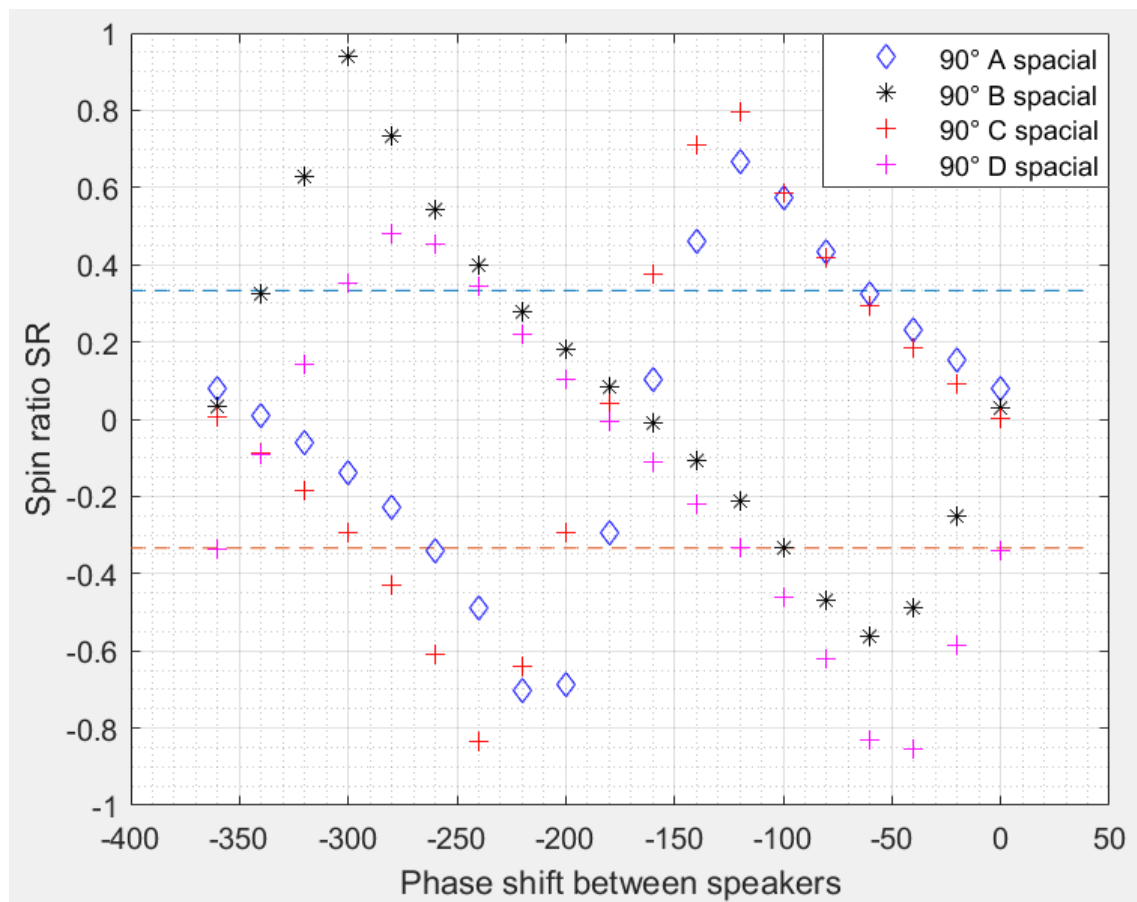


Figure 5.20: Spin ratio for different 90° positions and phases (same speakers)

Chapter 6

Conclusion

6.1 What do we know?

Most of the goals set for this thesis were achieved. A better understanding of spinning, standing and mixed modes was to be gained by acoustic means. The relative importance of forcing amplitude, phase and speaker position was tested in different setups.

In chapter 5 the excitation of standing and mixed modes was demonstrated. Even though a perfect spinning mode could not be generated, mixed modes with predominant spinning characteristics were demonstrated. The influence of amplitude, phase and speaker position were explored. The most promising control over the sound field seems to be a well chosen 135° speaker positioning, combined with a matching phase according to 5.16. Combined with the amplitude variation of both speakers it is possible to cover most of the surface in the amplitudes' scatterplot.

The influence of more than two speakers could not be investigated, as the behavior of two speakers was not yet fully understood.

6.2 What could be done next?

Further investigations could include a numerical model with acoustic loss, to compare with the measurement results. This would help to unveil the relative importance of acoustic losses, geometry and speaker influence. If following works would include finding two acoustic drivers behaving in a more predictable way, the number of error sources could be reduced.

If we look at the setup with four different 90° positions, it seems that some positions are preferable to others.

The author would therefore suggest investigations regarding:

- speaker influence: consider speaker calibration
- manufacturing tolerance: is the rig close enough to an ideal rig with 45° tubes, normal to the cylindrical surface?
- acoustic loss influence: how does the path ACW/CW spinning waves have to travel around the annulus, to reach the other speaker, influences their amplitude?
- more than two forcing speakers to find out if the response is smoothed

Lessons learned

The challenges of experimental work have been experienced during the preparation of this work. Time pressure, familiarizing with and limited availability of equipment are probably more common challenges and could not have been avoided.

However, making further measurements before the previous ones were fully evaluated and understood could have been avoided. Some experiment setups could have been designed better if the results of previous experiments would have been known at that time.

Likewise the importance of not varying too many parameters between measurements is now clearer to the author. The interpretation of the results would be easier and more informative if only one parameter (speaker, speaker position, microphone position) was varied at a time.

List of Figures

1.1	Scheme gas turbine [21]	1
1.2	Gas turbine architecture [9]	4
1.3	Coupling of acoustics and combustion [9]	9
1.4	Statistical prevalence illustrated [19]	13
1.5	Annular chamber with acoustic drivers as used in [20]	14
1.6	Annular chamber equipped several acoustic drivers, permitting to influence the spin ratio by shifting the phase between the signals of the drivers	16
2.1	Spacial heat release distribution in an annular combustion chamber [19]	18
2.2	Standing wave pressure distribution for various times [11]	20
2.3	Kundt's tube with reflecting end	20
2.4	Kundt's tube and two acoustic drivers	21
2.5	Analogy: the tube can be imagined as bowed, its ends connected. The result nearly is an annular chamber. The two microphone method can be applied in the same way as in the tube.	22
2.6	Kundt's tube with two acoustic drivers	24
2.7	Pressure time series at both locations x2 and x3 including gaussian noise	24
2.8	FFT of pressure time series	25
2.9	A and B determined using the two microphone method	26
2.10	Microphone position in pressure tapping	27

3.1	Experimental rig in sectional view as used for the current work. [19]	29
3.2	Speaker and microphone positions of the experimental rig in top view	31
3.3	The experimental setup: inputs and outputs	32
3.4	Experimental rig	35
4.1	LabVIEW block diagram	36
4.2	LabVIEW front panel	37
4.3	Detrending the signal (left) to eliminate the time-varying offset (right)	38
4.4	Stepwise treatment of the DFT signal: (top): DFT, (2nd): conversion to frequency, (3rd): unmirrored, (bottom): scaled	40
5.1	Mode characterisation: scatterplot amplitudes A and B	48
5.2	Mode characterisation: spin ratio	49
5.3	Setup for microphone calibration measurements	50
5.4	Scatterplot comparison: normal and with microphone calibration error	52
5.5	Spin ratio comparison: normal and with microphone calibration error	53
5.6	Setup for speaker calibration measurements	54
5.7	Frequency sweep, 100s, 200-2000Hz: FFT of pressure response	56
5.8	Frequency sweep in detail	57
5.9	Setup 90° between used speakers	58
5.10	Scatterplot for three different amplitudes (pointsize) and 10° phase steps	59
5.11	Spin ratio for three different amplitudes and 10° phase steps	60
5.12	Increasing the amplitude of one speaker: error due to speaker differences	61
5.13	Speaker positioning for current setup	62

5.14	Scatterplot for different speaker positions and phases between signals	63
5.15	Spin ration for different speaker positions and phases between signals	64
5.16	Scatterplot for different speaker positions and phases between signals (same speakers)	65
5.17	Spin ratio for different speaker positions and phases between signals (same speakers)	66
5.18	Different 90° speaker positions	67
5.19	Scatterplot for different 90° positions and phases (same speakers)	68
5.20	Spin ratio for different 90° positions and phases (same speakers)	69

List of Tables

2.1	Microphone comparison and error: each microphone's error is calculated relative to the mean value of the three microphones for different frequencies . . .	28
5.1	Microphone calibration results	51
5.2	Speaker calibration: error relative to mean pressure for each microphone . . .	55

Bibliography

- [1] M. Bauerheim and P. Salas. *Symmetry breaking of azimuthal thermoacoustic modes in annular chambers: a theoretical study*, 2014.
- [2] Jean-Francois Bourgouin and Durox Daniel. *Self-sustained instabilities in an annular combustor coupled by azimuthal and longitudinal acoustic modes*, 2013.
- [3] Anders Brandt. *Noise and vibration analysis*, 1 edition, 2011.
- [4] Brüel and Kjær. *BA721617 Measuring Microphones*.
- [5] Brüel and Kjær. *BR0047-13 Measuring Sound*.
- [6] Giulio Ghirardo and Matthew P. Juniper. *Azimuthal instabilities in annular combustors: standing and spinning modes*, 2013.
- [7] Horst Irretier. *Experimentelle Modalanalyse*, 4 edition, 2004.
- [8] T. P. Ivleva and A. G. Merzhanov. *Three dimensional spinning waves in the case of gas-free combustion*, 1999.
- [9] Arthur H. Lefebvre and Dilip R. Ballal. *Gas Turbine Combustion*, 3 edition, 2010.
- [10] B. J. Matkowsky and D. O. Olagunju. *Spinning Waves in Gaseous Combustion*, 1982.
- [11] Michael Möser. *Technische Akustik*, 9 edition, 2012.
- [12] M. Norambuena, A. Jakob, and M. Möser. *A Wave Decomposition Method for the Active Control of Sound Absorption*.
- [13] T. Poinso, P. Wolf, G. Staffelbach, L. Y. M. Gicquel, and J. D. Muller. *Identification of azimuthal modes in annular combustion chambers*, 2011.
- [14] Ernst Schneider. *Modellbasierte Regelung von Gasturbinenbrennkammern zur Optimierung von Stickoxidemissionen und Verbrennungsinstabilitäten*, 2009.

-
- [15] C. Sensiau and F. Nicoud. *Computation of azimuthal combustion instabilities in an helicopter combustion chamber*.
- [16] Poinsoit Thierry and Veynante Denis. *Theoretical and numerical combustion*, 2 edition, 2005.
- [17] Reinhard Willinger. *Thermische Turbomaschinen*, 2015.
- [18] P. Wolf and G. Staffelbach. *Azimuthal instabilities in annular combustion chambers*, 2010.
- [19] Nicholas A. Worth and James R. Dawson. *Modal dynamics of self-excited azimuthal instabilities in an annular combustion chamber*, 2013.
- [20] Nicholas A. Worth and James R. Dawson. *Azimuthally forced flames in an annular combustor (not published yet)*, 2015.
- [21] www.yourdictionary.com/gas-turbine (June 2016). *Gas turbine scheme*.

Appendices

Numerical model of the two microphone method

```
1 close all      % close all figure windows that are open
2 clear all     % clear all the variables currently stored in memory
3 clc          % clear the commands in the command window
4 format short g          %makes decimals visible as such
5 %-----
6 %FREQ, SPEED OF SOUND AND WAVENUMBER
7 f=765;          %frequency
8 c=343;          %speed of sound
9 k=2*pi*f/c;    %wave number
10 %-----
11 %AMPLITUDES AND MEASUREMENT POINTS
12 A=25;          %amplitude A
13 B=15;          %amplitude B
14
15 x2=0.15;       %measuring distances
16 x3=0;
17
18 fs=51200;      %sampling frequency
19 time=10;       %time of sampling
20
21 t=0:1/fs:time-1/fs; %time vector
22 %-----get pressure values at mic locations and add noise-----
23 mic2=pressurefunction_x_t_k_f_A_B(x2,t,k,f,A,B)+randn(1,fs.*time);
24 mic3=pressurefunction_x_t_k_f_A_B(x3,t,k,f,A,B)+randn(1,fs.*time);
25 %-----%real part microphones-----
26 %real part microphones
27 mic2_real=real(mic2);
28 mic3_real=real(mic3);
29 %-----plots pressure time series-----
30 subplot(2,1,1)
31 plot(t,mic2_real)
32 grid on
33 grid minor
```

```

34 title('Mic 2')
35 xlabel('Time (s)');
36 ylabel('Pressure (Pa)');
37 %--
38 subplot(2,1,2)
39 plot(t,mic3_real)
40 grid on
41 grid minor
42 title('Mic 3')
43 xlabel('Time (s)');
44 ylabel('Pressure (Pa)');
45 %-----FFT-----
46 N = length(mic2);
47 N_2 = ceil(N/2);
48
49 mic2_fft=fft(mic2)/N;      %FFT and scaling
50 mic3_fft=fft(mic3)/N;
51
52 mic2_fft_max=max(mic2_fft);
53 mic3_fft_max=max(mic3_fft);
54
55 [amplitudeA,amplitudeB]=calculate_back(mic3_fft_max,mic2_fft_max,x3,x2,k)
56 amplitudeA_abs=abs(amplitudeA)
57 amplitudeB_abs=abs(amplitudeB)
58 %-----plots FFT-----
59 figure
60 subplot(2,1,1)
61 bin_vals = [0 : N-1];      %adapt to frequency instead of bins
62 fax_Hz = bin_vals*fs/N;   %adapt to frequency instead of bins
63 N_2 = ceil(N/2);          %ceil rounds to next integer
64 plot(fax_Hz(1:N_2), abs(mic2_fft(1:N_2)))
65 xlabel('Frequency (Hz)')
66 ylabel('Magnitude (Pa)');
67 title('Magnitude spectrum (Hertz) Mic 2 FFT');
68 grid on
69 grid minor
70 %--

```

```

71 subplot(2,1,2)
72 bin_vals = [0 : N-1];
73 fax_Hz = bin_vals*fs/N;
74 N_2 = ceil(N/2);
75 plot(fax_Hz(1:N_2), abs(mic3_fft(1:N_2)))
76 xlabel('Frequency (Hz)')
77 ylabel('Magnitude (Pa)');
78 title('Magnitude spectrum (Hertz) Mic 3 FFT');
79 grid on
80 grid minor

```

This is how the “calculate back” function is defined:

```

1 function [amplitudeA,amplitudeB]=calculate_back(mic1,mic2,x1,x2,k)
2
3 amplitudeA=(mic2-mic1*exp(1i*k*(abs(x2-x1))))/(exp(-1i*k*(abs(x2-x1)))
4                                     -exp(1i*k*(abs(x2-x1))));
5 amplitudeB=-(mic2-mic1*exp(-1i*k*abs(x2-x1)))/(exp(-1i*k*(abs(x2-x1)))
6                                     -exp(1i*k*(abs(x2-x1))));
7 end

```

And this is what the “pressurefunction” function looks like:

```

1 function pressure=pressurefunction_x_t_k_f_A_B(x,t,k,f,A,B)
2 pressure=(A*exp(-1i*k*x)+B*exp(1i*k*x))*exp(1i*2*pi*f*t);
3 end

```